27. NAKAYAMA M, MANABE N, NISHIHARA S, MIYAMOTO H: Species-specific differences in apoptotic cell localization in granulosa and theca interna cells during follicular atresia in porcine and bovine ovaries. J Reprod Dev 46:147–156, 2000.
28. NAKAYAMA M, MANABE N, INOUE N, MATSUI T, MIYAMOTO H: Changes in the expression of tumor necrosis factor (TNF) α, TNFα receptor (TNFR) 2, and TNFR-associated factor 2 in granulosa cells during atresia in pig ovaries. Biol Reprod 68:530–535, 2003.
29. NIWA H: Molecular mechanism to maintain stem cell renewal of ES cells. Cell Struct Funct 26:137–148, 2001.
30. ODORICO JS, KAUFMAN DS, THOMSON JA: Multilineage differentiation from human embryonic stem cell lines. Stem Cells 19:193–204, 2001.
31. OLSON MV, VARKI A: Sequencing the chimpanzee genome: insights into human evolution and disease. Nat Rev Genet 4:20–28, 2003.
32. PADILLA SL, BAYATI J, GARCIA JE: Prognostic value of the early serum estradiol response to leuprolide acetate in in vitro fertilization. Fertil Steril 53:288–294, 1990.
33. PRANGE-KIEL J, KREUTZKAMM C, WEHRENBERG U, RUNE GM: Role of tumor necrosis factor in preovulatory follicles of swine. Biol Reprod 65:928–935, 2001.
34. REYNOLDS LP, GRAZUL-BILSKA AT, REDMER DA: Angiogenesis in the female reproductive organs: pathological implications. Int J Exp Pathol 83:151–163, 2002.
35. SAKAMAKI K, YOSHIDA H, NISHIMURA Y, NISHIKAWA S, MANABE N, YONEHARA S: Involvement of Fas antigen in ovarian follicular atresia and luteolysis. Mol Reprod Dev 47:11–18, 1997.
36. SCHIPPER I, HOP WCJ, FAUSER BCJM: The follicle-stimulating hormone (FSH) threshold/window concept examined by different interventions with exogenous FSH during the follicular phase of the normal menstrual cycle: duration, rather than magnitude, of FSH increase affects follicle development. J Clin Endocrinol Metab 83:1292–1298, 1998.
37. SHIMIZU K, DOUKE C, FUJITA S, MATSUZAWA T, TOMONAGA M, TANAKA M, MATSUBAYASHI K, HAYASHI M: Urinary steroids, FSH and CG measurements for monitoring the ovarian cycle and pregnancy in the chimpanzee. J Med Primatol 32:15–22, 2003.
38. SHIMODA K, SATO E, TANAKA T, TAKEYA T, TOYODA Y: Morphological differentiation of the microvasculature during follicular development, ovulation and luteinization of mouse ovaries. Dev Growth Differ 35:431–437, 1993.
39. STOUFFER RL, MARTINEZ-CHEQUER JC, MOLSKNESS TA, XU F, HAZZARD TM: Regulation and action of angiogenic factors in the primate ovary. Arch Med Res 32:567–575, 2001.
40. TILLY JL, KOWALSKI KI, JOHNSON AL, HSUEH JW: Involvement of apoptosis in ovarian follicular atresia and postovulatory regression. Endocrinology 129:2799–2801, 1991.
41. WADA S, MANABE N, INOUE N, NAKAYAMA M, MATSUI T, MIYAMOTO H: Trail-decoy receptor-1 disappears in granulosa cells of atretic follicles in porcine ovaries. J Reprod Dev 48:167–173, 2002.
42. WADA S, MANABE N, INOUE N, NAKAYAMA M, MATSUI T, MIYAMOTO H: TRADD is involved in apoptosis induction in granulosa cells during atresia in pig ovaries. J Reprod Dev 48:175–181, 2002.
43. WANG TH, HORNG SG, CHANG CL, WU HM, TSAI YJ, WANG HS, SOONG YK: Human chorionic gonadotropin-induced ovarian hyperstimulation syndrome is associated with up-regulation of vascular endothelial growth factor. J Clin Endocrinol Metab 87:3300–3308, 2002.
44. WOBUS AM: Potential of embryonic stem cells. Mol Aspects Med 22:149–164, 2001.
45. YANO J, NODA Y, IDA K, MORI T, GOULD KG: In vitro fertilization and embryo transfer in the chimpanzee. Jpn J Fertil Streril 33:169–173, 1988 [in Japanese].
46. ZELINSKI-WOOTEN MB, HUTCHISON JS, HESS DL, WOLF DP, STOUFFER RL: Follicle stimulating hormone alone supports follicle growth and oocyte development in gonadotropin-releasing hormone antagonist-treated monkeys. Hum Reprod 10:1658–1666, 1995.

Develop. Growth Differ. (2005) **47**, 163–172

Characterization of an exchangeable gene trap using pU-17 carrying a stop codon-*βgeo* cassette

Takuya Taniwaki,[1] Kyoko Haruna,[1,3] Hiroshi Nakamura,[1,3] Tomohisa Sekimoto,[1] Yuichi Oike,[1] Takashi Imaizumi,[1] Fumiyo Saito,[1] Mayumi Muta,[1] Yumi Soejima,[1,3] Ayako Utoh,[1,3] Naomi Nakagata,[2] Masatake Araki,[2] Ken-ichi Yamamura[1,3,*] and Kimi Araki[1,*]

[1]*Institute of Molecular Embryology and Genetics, Kumamoto University, Kuhonji 4-24-1, Kumamoto 862-0976, Japan,* [2]*Institute of Resource Development and Analysis, Kumamoto University, Honjo 2-2-1, Kumamoto 860-0811, Japan, and* [3]*TransGenic, 1155-5 Tabaru, Mashiki-machi, Kumamoto 861-2202, Japan*

We have developed a new exchangeable gene trap vector, pU-17, carrying the intron-*lox*71-splicing acceptor (SA)-*βgeo-lox*P-pA-*lox*2272-pSP73-*lox*511. The SA contains three stop codons in-frame with the ATG of *βgalactosidase/neomycin-resistance fusion* gene (*βgeo*) that can function in promoter trapping. We found that the trap vector was highly selective for integrations in the introns adjacent to the exon containing the start codon. Furthermore, by using the Cre-mutant *lox* system, we successfully replaced the *βgeo* gene with the *enhanced green fluorescent protein* (*EGFP*) gene, established mouse lines with the replaced clones, removed the selection marker gene by mating with Flp-deleter mice, and confirmed that the replaced *EGFP* gene was expressed in the same pattern as the *βgeo* gene. Thus, using this pU-17 trap vector, we can initially carry out random mutagenesis, and then convert it to a gain-of-function mutation by replacing the *βgeo* gene with any gene of interest to be expressed under the control of the trapped promoter through Cre-mediated recombination.

Key words: Cre/*lox*, embryonic stem cell, Flp/*FRT*, gene trap, site-specific recombination.

Introduction

The whole human and mouse genome sequences are now near to completion (Waterston *et al.* 2002). However, gene functions *in vivo* cannot be understood from the sequence information alone, and mutational analysis is a powerful and efficient approach for studying functional genomics. Gene trapping in embryonic stem (ES) cells is a proven method for isolating large numbers of random insertional mutations that can be easily identified (Gossler *et al.* 1989; Gossler 1993; Evans *et al.* 1997; Zambrowicz & Friedrich 1998; Stanford *et al.* 2001; Hansen *et al.* 2003; Stryke *et al.* 2003). Gene trap vectors contain a promoter-less reporter gene downstream of a splice acceptor (SA) and a selectable marker gene. When the gene trap vector is introduced and integrated into endogenous genes, a fusion transcript between the endogenous gene and the reporter gene is produced, such that the expression of the trapped gene can be monitored. Both the trapped cDNA and the genomic site of the integration can easily be cloned by rapid amplification of cDNA 5′-ends (5′-RACE) (Townley *et al.* 1997) and the plasmid rescue method (Araki *et al.* 1999). To date, trap vectors carrying the internal ribosomal entry site (IRES) from the encephalomyocarditis virus (ECMV) (Jang & Wimmer 1990; Ghattas *et al.* 1991; Mountford & Smith 1995; Kang *et al.* 1997) and the *βgalactosidase/neomycin-resistance fusion* gene (*βgeo*) (Friedrich & Soriano 1991; Voss *et al.* 1998) have been widely used and proven to trap various genes expressed in ES cells (Chowdhury *et al.* 1997; Bonaldo *et al.* 1998; Stoykova *et al.* 1998).

In typical gene trapping, insertion of a trap vector can only induce truncation mutations. In order to change the trapped alleles into a more subtle mutation, such as a point mutation, we previously developed a site-directed integration system in ES cells using the Cre-LE/RE mutant *lox* system (Araki *et al.* 1997), and constructed an exchangeable gene trap vector, pU-Hachi, carrying SA-*lox*71-IRES-*βgeo*–polyadenylation signal (pA)-*lox*P-pA-pUC (Araki *et al.* 1999). The *βgeo* gene in pU-Hachi trap clones can be replaced with any other cDNA of interest through Cre-mediated integration.

*To whom correspondence should be addressed.
Email: arakimi@gpo.kumamoto-u.ac.jp, yamamura@gpo.kumamoto-u.ac.jp
Received 27 November 2004; revised 30 January 2005; accepted 3 February 2005.

Therefore, we can carry out random insertional mutagenesis as the first step, and then introduce cDNA fragments for expression in the same pattern as the *βgeo* in the second step. Thus, we can also utilize trap clones as promoter resources.

However, there are several limitations to replacement experiments using pU-Hachi. First, the SA and *lox*71 sequences contain 4 and 1 stop codon(s), respectively. Hence, if a genomic gene carrying both exons and introns is inserted into the *lox*71 site, the stop codons present in the SA become premature translation termination codons, leading to nonsense codon-mediated mRNA decay (NMD) (Wagner & Lykke-Andersen 2002). Second, because the IRES is used for cap-independent translation of the *βgeo* gene, it is necessary to use the IRES for translation of the inserted cDNA and this makes the construction of replacement vectors laborious. Third, trap vectors containing the IRES often integrate into the 3′ region of a gene resulting in the production of a truncated form, which could modify the phenotype (Oike *et al.* 1999). Fourth, the 3′-part of the trapped gene cannot be reutilized, because the pA sequence is located outside the floxed region and cannot be removed. For example, we have tried 3′-rapid amplification of cDNA ends by inserting a promoter sequence, but no transcripts fused to the 3′-part of the trapped gene were produced. Fifth, it is difficult to insert and express the *cre* gene, because a re-excision reaction sometimes occurs in the LE/RE mutant *lox* system (Albert *et al.* 1995).

Recently, we showed that combination of the LE/RE mutant *lox* with a heterospecific *lox*, *lox*2272, improved the recombination efficiency and made it possible to integrate the *cre* gene through recombination by Cre (Araki *et al.* 2002). Based on these findings, we have constructed a new gene trap vector suitable for the insertion and expression of cDNA, genomic DNA and the *cre* gene. The new gene trap vector, pU-17, was designed to be a promoter trap and carried 3 kinds of mutant *lox* sites for replacement. We demonstrate here that pU-17 is efficiently integrated around the initiation codon, the *βgeo* gene is easily replaced with the *enhanced green fluorescent protein* (*EGFP*) gene, and the same expression pattern *in vivo* is maintained after the replacement.

Materials and Methods

Plasmids

The trap vectors pU-17 and pU-18 were constructed from the pU-Hachi vector by several modifications (Araki *et al.* 1999):

1. The *lox*71 site was inserted to the 5′-side, within the intron sequence of the mouse *En-2* gene.
2. The polyadenylation (pA) signal of the βgeo gene was removed.
3. A *lox*2272 sequence was inserted in front of the pA signal of the mouse *phosphoglycerate kinase-1* (*Pgk*) gene.
4. The pSP73 (Promega, Madison, WI, USA) vector was used instead of the pUC vector in pU-Hachi.
5. The IRES sequence was removed. The vectors were linearized at their single *Spe*I site before electroporation.

The Cre expression vector, pCAGGS-Cre, was described previously (Araki *et al.* 1995; Araki *et al.* 1997). The plasmid pCAGGS-Flp was constructed by ligating fragments of the *Flp* gene (Stratagene, La Jolla, CA, USA) into the *Eco*RI sites of pCAGGS. The mutation in the *Flp* gene (Ringrose *et al.* 1998) was corrected.

The replacement vector, p6SEFPPF, was assembled from components of pSP73 (Promega), the *lox* 66 sequence, the *EGFP* gene (Clontech, Palo Alto, CA, USA), the *FRT* sequence, the *Pgk* promoter, the *puromycin N-acetyltransferase* (*Pac*) gene and the *lox*P sequence.

Cell culture and electroporation

The ES cell lines TT2 (Yagi *et al.* 1993) and E14tg2a (Niwa *et al.* 2002) were grown as described. For electroporation with the pU-17 and pU-18 gene trap vectors, 80 μg of *Spe*I-digested DNA and 2×10^7 cells were used. The cells were suspended in 0.8 mL of phosphate-buffered saline (PBS), electroporated using a Bio-Rad Gene Pulser (Bio-Rad Laboratories, Hercules, CA, USA) set at 800 V and 3 μF, and then fed with medium supplemented with 200 μg/mL of G418 after 48 h. Selection was maintained for 7 days, and the colonies were then counted, picked and placed in 24-well plates. Replacement by Cre-mediated recombination in ES cells was performed as described previously (Araki *et al.* 1999).

Analyses of genomic DNA

Cells or tissues were lysed with sodium dodecylsulfate (SDS)/proteinase K, treated with 1:1 (v/v) phenol/chloroform, precipitated with ethanol, and dissolved in 10 mM Tris-HCl, pH 7.5/1 mM ethylenediamine tetraacetic acid (EDTA) (TE). Six micrograms of genomic DNA was digested with appropriate restriction enzymes, electrophoresed in a 0.9% agarose gel and then blotted onto a nylon membrane

(Roche Diagnostics, Basel, Switzerland). Hybridization was performed using a DIG DNA Labeling Kit (Roche).

For polymerase chain reaction (PCR) analysis, DNA (50 ng) were subjected to 30 cycles of amplification (with each cycle consisting of 1 min at 94°C, 2 min at 55°C and 2 min at 72°C) in a thermal cycler. The primer sequences were as follows: for detection of the recombined allele, SA5 (5′-GGTCACTTTATGTTCTTGCCC-3′) and GFP2 (5′-TGTGATCGCCGTTCTCGTTG-3′); for detection of the *βgeo* sequence, Z1 (5′-GCGTTACCCAACTTAATCG-3′) and Z2 (5′-TGTGAGCGAGTAACAACC-3′); for detection of the *CAGGS-Flp* transgene, AG2 (5′-CTGCTAACCATGTTCATGCC-3′) and Flp5 (5′-ATCCTACCCCTTGCGCTAAA-3′).

RNA analyses

Total RNA was isolated from ES cells using Sepasol (Nakalai, Kyoto, Japan). Ten micrograms of total RNA was electrophoresed through 1.0% agarose-formaldehyde gels and transferred to a positively charged nylon membrane (Roche). After baking at 80°C for 1 h, the membrane was prehybridized, and then hybridized with RNA probes prepared using a DIG RNA Labeling and Detection Kit (Roche).

Five micrograms of total RNA was used for first-strand cDNA synthesis with the reverse transcriptase ReverScript (Wako Pure Chemical Industries, Osaka, Japan) and the LZUS3 primer (5′-GCGCATCGTAACCGTGCAT-3′) in the lacZ sequence. 5′-RACE was performed using the 5′-RACE system (Invitrogen, Carlsbad, CA, USA) according to the manufacturer's instructions. The initial PCR was performed using the primer SA13 (5′-TCTGAAACTCAGCCTTGAGC-3′) in the SA sequence and the anchor primer (5′-GGCCACGCGTCGACTAGTACGGGiiGGGiiGGGiiG-3′) (Invitrogen). Next, nested PCR was performed using the primer SA10 (5′-AGCAGTGAAGGCTGTGCGA-3′) in the SA sequence and the amplification primer (5′-GGCCACGCGTCGACTAGTAC-3′) in the anchor primer sequence. The PCR product was electrophoresed, purified with Quantum Prep Freeze 'N Squeeze DNA Gel Extraction Spin Columns (Bio-Rad), and sequenced by the dideoxy-chain termination method using a Big Dye Terminator Cycle Sequencing kit (Perkin Elmer, Foster City, CA, USA). All the obtained sequences were confirmed by RT-PCR using first-strand cDNA synthesized with random primers. The obtained sequences were compared with the GenBank and GenEMBL databases using the BLASTN program (http://blast.genome.jp) (Altschul *et al.* 1990), and the exon-intron structures were examined using the Celera Discovery System (Applied Biosystems Japan, Tokyo, Japan).

Production of chimeric mice and microinjection

Chimeric mice were produced by aggregation of ES cells with eight-cell embryos of ICR mice (CLEA Japan, Tokyo, Japan). Chimeric male mice were mated with C57BL/6 J females (CLEA Japan) to obtain F1 heterozygotes.

For microinjection of CAGGS-Flp, superovulated BDF1 (Charles River, Osaka, Japan) females were mated with BDF1 males. Fertilized eggs were collected and pronuclear injection was performed according to a previously described procedure (Yamamura *et al.* 1984).

Histological analysis

For 5-bromo-4-chloro-3-indolyl β-D-galactopyranoside (X-gal) staining, tissues were fixed in 4% paraformaldehyde for 6 h, sectioned with a vibratome at 50 μm, treated with 1% Triton X-100 in PBS for 10 min, washed three times in PBS, incubated overnight at 30°C in staining solution (5 mM potassium ferricyanide, 5 mM potassium ferrocyanide, 2 mM $MgCl_2$, 0.5% X-gal in PBS), mounted on glass slides, and counterstained with Nuclear Fast red. For immunohistochemistry, paraffin sections were prepared and stained with an anti-EGFP rabbit polyclonal antibody (MBL, Nagoya, Japan).

Results

Construction of pU-17

The structure of pU-17 is shown in Figure 1(A). The improvements from pU-Hachi are as follows:

1. A *lox*71 site was inserted into the intron sequence of the SA.
2. *Lox*2272 and *lox*511 sites were inserted into the downstream of the pA and plasmid vector tail, respectively. Through these two alterations, various replacements became possible (see Fig. 5 and Discussion).
3. The IRES was removed, and as a result, the three stop codons in the exon sequence of the SA were in-frame with the ATG of the *βgeo* gene (Fig. 1C). It is theoretically expected that only clones in which the vector is integrated into the upstream of the start codon of a trapped gene will become neo-resistant. Thus, this Stop-*βgeo* vector is expected to function in promoter trapping, and should be ideal for expressing cDNA under the control of a trapped gene. However, this restriction of the integration site may result in a reduction in the colony formation efficiency. Therefore, we examined the colony formation efficiency of pU-17 by comparison with a trap vector using the IRES of ECMV.

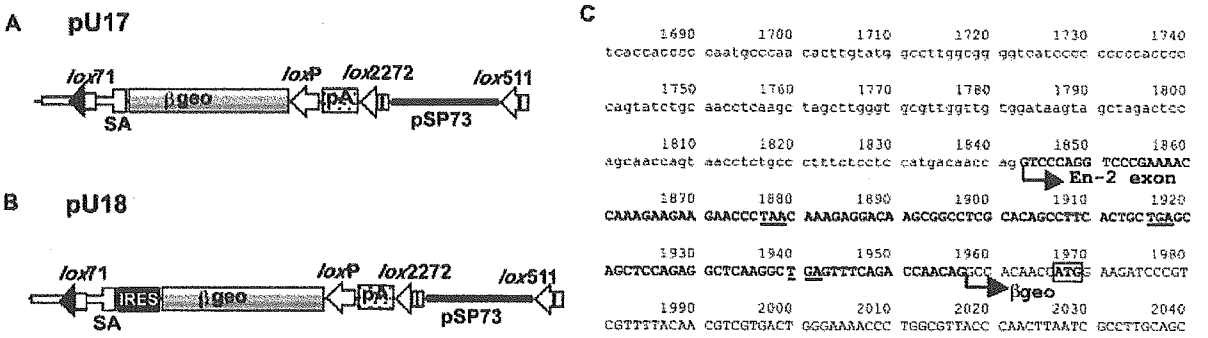

Fig. 1. Structure of the gene trap vectors. (a) Schematic representation of the trap vector pU-17. pU-17 contains 1.8 kb of an intron and a splice acceptor (SA) sequence from the mouse *En-2* gene, the *βgeo* gene and a polyadenylation signal (pA). A *lox*71 site is located within the intron sequence, and *lox*P, *lox*2272 and *lox*511 sites are placed in the downstream of the *βgeo*, pA and pSP73 vector sequences, respectively. (b) Schematic representation of the trap vector pU-18. The only difference between pU-17 and pU-18 is the presence of the internal ribosomal entry site (IRES) sequence of encephalomyocarditis virus (ECMV) between the SA and *βgeo*. (c) Sequence of the junction of the SA and the *βgeo* gene of pU-17. Lower and upper case letters represent the intron and exon sequences, respectively. There are three in-frame stop codons (underlined) in the upstream of the *βgeo* initiation codon (boxed). It is theoretically expected that the integration site of the vector should be restricted to the upstream of the start codon of a trapped gene.

Table 1. Colony formation efficiencies of pU-17 and pU-18

Trap vector	Number of G418-resistant colonies 1st exp.	2nd exp.	3rd exp.
pU-17	34	135	36
pU-18	38	153	42

Eighty micrograms of linearized trap vector was introduced into 2×10^7 E14Tg2a cells. The electroporated cells were plated onto three 10 cm dishes and selected with G418 for 1 week, before the number of colonies was counted.

pU-17 has comparable colony formation efficiency to a trap vector containing an IRES

We constructed the pU-18 vector (Fig. 1B) carrying the IRES between the SA and *βgeo*. The only difference between pU-17 and pU-18 is the absence and presence of the IRES, respectively. In pU-18, a fusion message of the trapped gene and IRES-*βgeo* is produced, and translation starts from the AUG of both the trapped gene and *βgeo*. Therefore, trap clones should be G418-resistant independent of the insertion sites of the IRES-*βgeo* vector within the trapped genes (Bonaldo *et al.* 1998). The two vectors were introduced into ES cells harvested on the same day through electroporation. The cells were then selected with G418, and the numbers of colonies were counted. As shown in Table 1, almost the same numbers of colonies appeared with both vectors, indicating that the pU-17 Stop-*βgeo* vector has comparable colony formation efficiency to pU-18.

pU-17 integrates into the 5′-region of trapped genes

In order to examine the integration sites of pU-17 in trap clones, we first performed Northern blotting using randomly chosen pU-17 and pU-18 trap clones to compare the sizes of the fusion messages. If pU-17 integrates in the upstream of the start codon of a trapped gene, the lengths of trapped mRNA fused to *βgeo* should be short and therefore the total lengths of the fusion messages in pU-17 clones should be about 4.5 kb, corresponding to the length of SA-*βgeo*-pA. As shown in Figure 2(A), the sizes of the fusion messages in pU-17 clones were similar, spanning approximately 4.5–5 kb. On the other hand, various sizes of bands, most of which exceeded 5 kb, were detected in pU-18 clones, suggesting integration in the middle or 3′-half of the genes. This result indicates that pU-17 tends to integrate into the 5′-region of endogenous genes.

Next, to precisely analyze the insertion events in a larger number of trapped clones, trapped genes containing the pU-17 vector were determined by 5′-RACE analysis, and the results are summarized in Table 2. Regarding the 22 clones in which pU-17 was integrated into known genes, the integration sites in the context of their exon-intron structures were determined using the Celera Discovery System. As shown Figure 2(B), in 82% of the trap clones, pU-17 was integrated into the introns adjacent to the exon containing the start codon of the trapped gene. This results indicates that the pU-17 functions efficiently as a promoter trap vector.

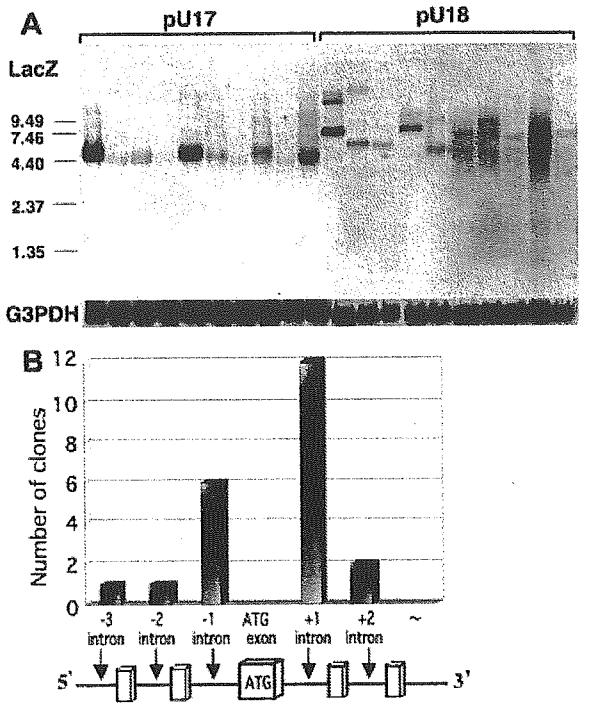

Fig. 2. (a) Northern blot analysis of trapped clones obtained using pU-17 (left) and pU-18 (right). RNA were prepared from embryonic stem (ES) clones carrying a single copy of the trap vector, and subjected to Northern blotting with a *LacZ* probe (upper) or *G3pdh* probe (lower). Size markers are shown on the left. (b) Histogram of the integration sites. Twenty-two clones in which a known gene was trapped were chosen, and the integration sites in the trapped genes were analyzed using the Celera Discovery System.

Table 2. Summary of the 5′-rapid amplification of cDNA ends (RACE) analysis results

Known	EST	Novel	ND†	Total
22 (17%)	61 (47%)	29 (22%)	17 (13%)	129 (100%)

The sequences obtained through 5′-RACE were compared to the published sequences in GenBank and the Celera Discovery System. †Not Determined: no product was obtained or part of the vector sequence (in many cases, the 5′-region of the intron sequence) was obtained.

Replacement of the βgeo gene with the EGFP gene

pU-17 carries four *lox* sites, such that the DNA sequence between *lox*71 and the other *lox* sites of *lox*P, *lox*2272 and *lox*511 can be replaced with another DNA sequence. To demonstrate the ability of pU-17 for such replacement, we performed targeted integration of the *EGFP* gene, as outlined in Figure 3. We constructed a replacement vector carrying a *lox*66-SA-*EGFP-FRT-Pgk* promoter-*Pac-FRT-lox*P-pSP73. For the targeted replacement, 20 μg of each targeting plasmid and pCAGGS-Cre were electroporated into trap ES clones in their circular forms. Because the replacement vector and trap vector in the genome carry two *lox* sites with the same spacer region (*lox*66 and *lox*P, and *lox*71 and *lox*P, respectively), it is expected that intramolecular recombination should initially occur between the two *lox* sites after co-electroporation, resulting in the production of two intermediate molecules, as shown in the middle of Figure 3. Next, the ES cells in which targeted replacement has occurred were selected in the presence of puromycin. Because the *Pac* gene in the targeting vector does not have a pA signal, random integrants should be puromycin sensitive, and only upon Cre-mediated targeted integration, the *Pac* gene fuses to the pA signal on the trap vector, thereby making the cells drug-resistant. After removal of the *Pac* gene using the Flp/*FRT* system, the *EGFP* gene is expressed under the control of the trapped promoter. This removal is achieved by mating with *CAGGS-Flp* transgenic mice.

Two trap clones were used for the replacement experiment. The Ayu17–71 clone has trapped a novel gene and the expression pattern of the *βgeo* is ubiquitous (see Fig. 4). The Ayu17–104 clone has trapped the *Shroom* gene (Hildebrand & Soriano 1999) and shows a tissue-specific expression pattern.

After electroporation, 17 and 16 colonies from Ayu17–71 and Ayu17–104, respectively, were picked, expanded and analyzed for recombination events. To confirm the 5′- and 3′-junctions, we performed PCR and Southern blot hybridization with the Pac probe, respectively. Targeted insertion should give a 1.5 kb band in the PCR and a 2.4 kb band in the Southern blotting (Fig. 3A). Figure 3(B) shows the results for Ayu17–104 subclones, of which 15 of 16 clones (94%) revealed the pattern of targeted replacement. Ayu17–71 subclones also showed a high targeting frequency of 82% (Table 3). These results demonstrate that the replacement system using poly(A) trapping functions efficiently.

Germline transmission of the replaced clones and mating with CAGGS-Flp mice

We produced chimeric mice using two replaced clones derived from each of the parental Ayu17–71 and Ayu17–104 lines, and successfully obtained germline chimeras from all the subclones used. Next, the chimeric male mice were mated with *CAGGS-Flp* transgenic mice which express the *Flp* gene ubiquitously (data not shown). In the double-positive mice for the *CAGGS-Flp* transgene and the replaced trap vector,

recombination should occur between the *FRT* sites, resulting in deletion of the PGK-pac sequence. We confirmed the recombination using tail DNA from the double-transgenic mice and Southern blotting with the *EGFP* probe. The recombined allele gives a 1.4 kb band, whereas the original allele gives a 2.8 kb band. As shown in Figure 3, the expected 1.4 kb band was obtained in the all double-transgenic mice. However, only 40–80% of the progenies from the double-transgenic mice showed the recombined pattern (data not shown), indicating that the *Flp* gene is not expressed in all the germ cells in this *CAGGS-Flp* transgenic line.

Expression pattern of the integrated EGFP gene

The *in vivo* expression pattern of the targeted integrated *EGFP* gene should be identical to that of the *βgeo* gene expression in the parental lines. First, we

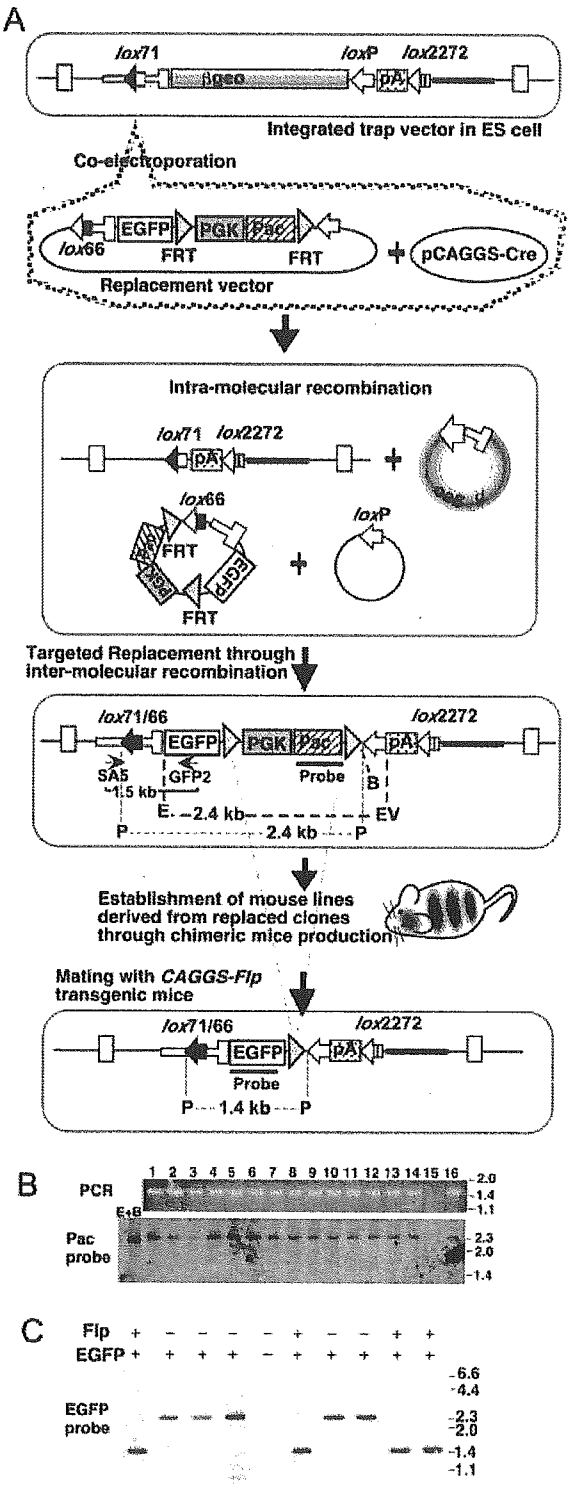

Fig. 3. Replacement of *βgeo* with *enhanced green fluorescent protein* (*EGFP*) and removal of the marker gene using the Flp/*FRT* system. (a) Scheme of the gene replacement. The structures of the integrated trap vector and targeting vector plasmid are shown in the top panel. The targeting vector p6SEFPPF carries *lox*66-SA-*EGFP-FRT-Pgk* promoter-*Pac-FRT-lox*P-pSP73. p6SEFPPF and the Cre-expression vector, pCAGGS-Cre, are co-electroporated into trap ES cells, and targeted recombinant cells are selected with puromycin. The expected intermediates produced through intermolecular recombination are shown in the second panel, followed by the allele replaced with the *EGFP* gene through Cre-mediated recombination. After establishment of a mouse line from the replaced clone, the selectable marker gene, *Pgk-Pac*, is removed by Flp/*FRT* recombination through mating with *CAGGS-Flp* transgenic mice. The recombined allele by Flp recombinase is shown in the bottom panel. The positions of the primers SA5 and GFP2, and the EGFP and Pac probes used for the Southern blotting are indicated by arrows and solid bars labeled 'probe', respectively. The expected sizes of the polymerase chain reaction (PCR) products and signals in Southern blotting are also indicated. E, *Eco*RI; EV, *Eco*RV; B, *Bam*HI; P, *Pst*I. (b) PCR and Southern blot analysis to detect targeted integration of the SA-*EGFP-FRT-Pgk-Pac-FRT* unit in subclones of Ayu17–104. Genomic DNA from 16 randomly picked subclones were subjected to PCR with SA5 and GFP2 to detect their 5′-junctions. For detection of their 3′-junctions, the genomic DNA were digested with *Eco*RV and *Eco*RI and hybridized with the Pac probe. Fifteen of 16 clones showed the expected pattern of targeted replacement, namely 1.5 kb in PCR and 2.4 kb in Southern blotting. The E + B lane represents *Eco*RI and *Bam*HI digestion, which should give 2.3 kb regardless of the integration position. (c) Detection of recombination by Flp recombinase. Genomic tail DNA of F1 offspring obtained from mating of chimeric male mice and *CAGGS-Flp* female transgenic mice were prepared and examined for the existence of the replaced allele and the *CAGGS-Flp* transgene by PCR. The PCR results are indicated at the top by a plus or minus. Next, the DNA were digested by *Pst*I and hybridized with the *EGFP* probe to detect recombination between FRT sites. Recombined alleles should give a 1.4 kb band, whereas unrecombined alleles should produce a 2.8 kb band. In all the double-transgenic mice, a 1.4 kb band is detected, indicating deletion of the PGK-Pac sequence through recombination by Flp.

Table 3. Results of targeted replacement with the *EGFP* gene

Parental cell line	Total no. of colonies	No. of colonies analyzed	No. of colonies with targeted integration	% of targeted integration
Ayu17–71	22	17	14	82
Ayu17–104	109	16	15	94

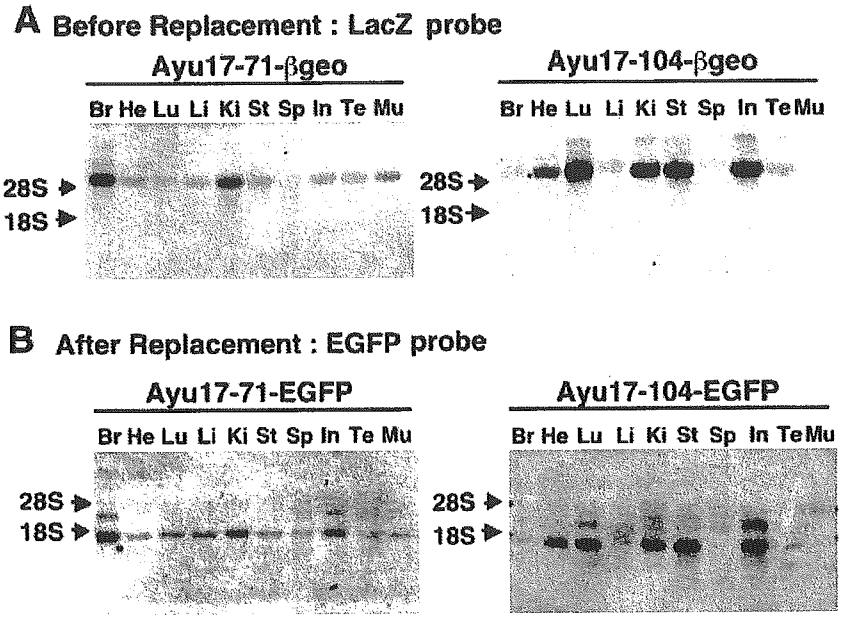

Fig. 4. Expressions of the *βgeo* and *EGFP* genes. (A) Northern blot analysis with the *LacZ* probe. Total RNA were extracted from tissues of adult hemizygous *Ayu17–71-βgeo* or *Ayu17–104-βgeo* trap mice, that had been established from parental trap clones carrying the *βgeo* gene, and subjected to Northern blotting. (B) Northern blot analysis with the *EGFP* probe. Double-positive F1 mice of the trap allele replaced with the *EGFP* gene and the *CAGGS-Flp* transgene were used. Br, brain; He, heart; Lu, lung; Li, liver; Ki, kidney; St, stomach; Sp, spleen; In, intestine; Te, testis; Mu, muscle.

examined the expression pattern by Northern blotting. Figure 4(A) shows the *βgeo* expression in heterozygous mice established from the parental trap lines before replacement, and Figure 4(B) shows the *EGFP* expression in double-positive F1 mice for the replaced trap allele and the *CAGGS-Flp* transgene. In the *Ayu17–71* line, *βgeo* expression was ubiquitous, but the brain and kidneys showed stronger expression. After replacement, the same expression pattern was observed for the *EGFP* gene. In the *Ayu17–104* line, *βgeo* expression was detected in the heart, lungs, kidneys, stomach and intestine, and the integrated *EGFP* gene showed the same expression pattern. In several tissues, extra bands of about 2.4 kb were detected. This size was identical to the size observed in the single-positive *EGFP* mice before recombination by Flp (data not shown), indicating that the recombination by Flp was not complete.

Next, we further confirmed the expression pattern at the cellular level by histological analysis with X-gal staining in the parental *βgeo* lines and immunostaining with an anti-EGFP antibody in the replaced *EGFP* lines. As shown in Figure 5, positive signals in the Purkinje cells, cerebrum and renal medulla in the *Ayu17–71* line (Fig. 5A) and the mucosa of the stomach and the glomerulus of the kidney in the *Ayu17–104* line (Fig. 5B) were detected in both staining procedures. Thus, the inserted *EGFP* gene was expressed with the same cell-type specific pattern as the original *βgeo* gene.

Discussion

Here, we have demonstrated that our exchangeable promoter trap system functioned as expected, in that the trap vector was selectively inserted into the 5′-region of endogenous genes, the *βgeo* reporter gene was easily replaced with another gene and, importantly, the inserted gene was expressed in the same pattern as the *βgeo* gene *in vivo*.

In addition to replacement of the reporter gene, many other replacements can be performed using the pU-17 trap clones, as shown in Figure 6. First, any genomic DNA or cDNA of interest can be expressed through replacement between *lox*71 and *lox*P (Fig. 6A). We can also introduce any type of mutation, such as a point or dominant-negative mutation. Second, through replacement between *lox*71 and *lox*2272, the *cre* gene can also be inserted and

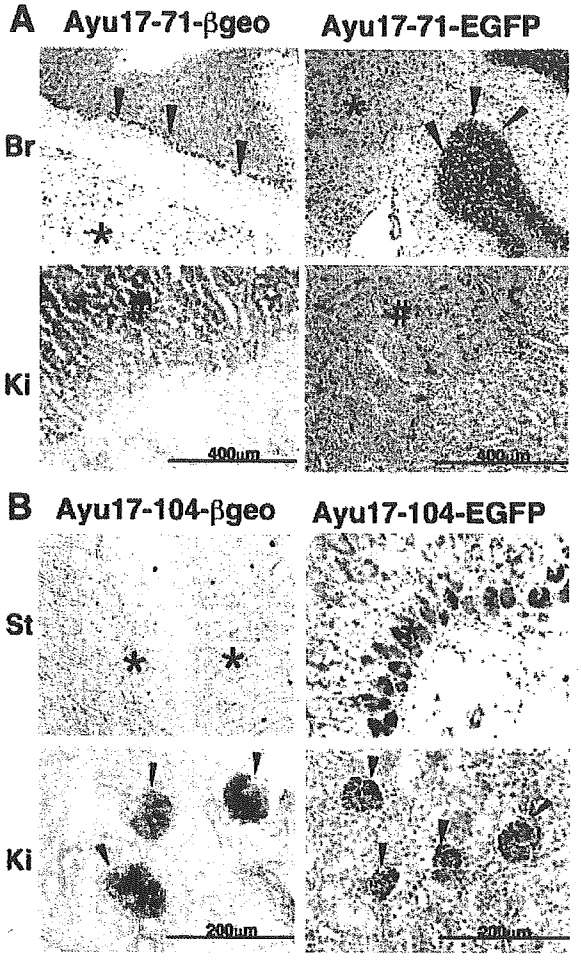

Fig. 5. Histological analysis of the expressions of the *βgeo* and *EGFP* genes. (a) The brain (Br) and kidney (Ki) from original *Ayu17–71-βgeo* and replaced *Ayu17–71-EGFP* mice were stained with X-gal (left) and an anti-EGFP antibody (right), respectively. In both staining procedures, positive signals are detected in the Purkinje cells (arrow heads), cerebrum (*) and renal medulla (#). (b) The stomach (St) and kidney (Ki) from original *Ayu17–104-βgeo* and replaced *Ayu17–104-EGFP* mice were stained with X-gal (left) and an anti-EGFP antibody (right), respectively. In both staining procedures, positive signals are detected in the mucosa of the stomach (*) and glomerulus of the kidney (arrow heads).

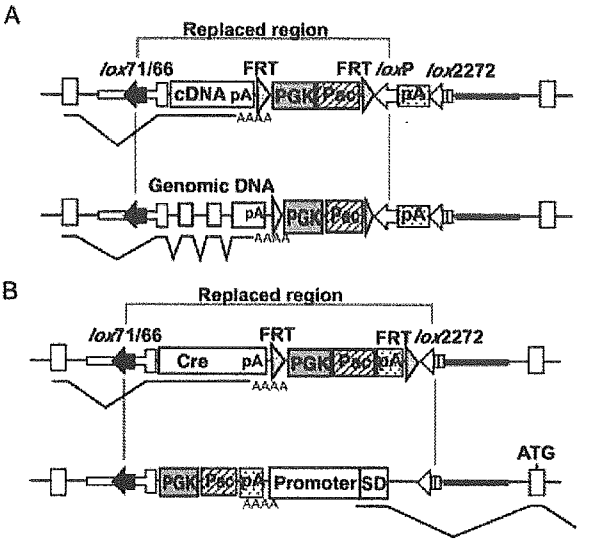

Fig. 6. Replacement patterns in trap clones with pU-17. (a) Replacement between *lox*71 and *lox*P. Any cDNA (upper) or genomic DNA (lower) of interest can be inserted and expressed under the control of the trapped promoter activity. (b) Replacement between *lox*71 and *lox*2272. The *cre* gene can also be expressed under the control of the trapped promoter activity (upper). If a promoter sequence followed by a splice donor site (SD) is inserted, it is possible to change the expression pattern of the trapped gene.

expressed (Fig. 6B, upper) as described previously (Araki *et al.* 2002). Because we can choose trap lines with the desired expression pattern by observing the *βgeo* expression, this should be convenient for the production of various Cre-mice. Third, in cases of integration of the trap vector into the 5′-region of the endogenous ATG, we can alter the expression pattern of the trapped gene by inserting an exogenous promoter (Fig. 6B, lower). By using a strong promoter in ES cells, this would be useful for 3′-RACE to determine the trapped gene when 5′-RACE fails or only produces quite a short sequence. In all cases, the selection marker gene used for replacement can be removed through mating with *CAGGS-Flp* mice.

In the pU-17 vector, we inserted in-frame stop codons in the upstream of the ATG of the *βgeo* gene for the convenience being able to express the inserted cDNA after replacement. It is not necessary to use the IRES or adjust the reading frames between the trapped gene and the inserted cDNA for this expression. Theoretically, this should reduce the colony formation efficiency, but our results revealed no significant differences in the colony formation efficiencies between vectors with and without IRES. We confirmed that the vector integration sites in pU-18 clones were completely random (data not shown), indicating that the IRES in pU-18 functioned as expected in the trap clones. We suppose that IRES-dependent translation is affected by the surrounding sequence and cannot always start efficiently. On the other hand, Bonaldo *et al.* (1998) reported that their SA-IRES-*βgeo* vector showed 6.7-fold higher colony formation efficiency than their SA-*βgeo* vector. Although the reason for this result is not clear, it would be due to the absence of the start codon of the *βgeo* in their SA-*βgeo* vector. With their vector,

therefore, trap clones become G418 resistant only when a stable and active fusion protein of the *βgeo* and trapped gene is produced from the trapped allele. We speculate that the probability of the production of active fusion protein would be much lower than that of successful trap event with pU-17.

The trap vector pU-17 showed a strong bias to integration into the 5′-region of the genes. It is well known that retroviral vectors show a tendency for integration into the 5′-end of genes (Friedrich & Soriano 1991; von Melchner *et al.* 1992), but no plasmid trap vectors have been reported to have such a tendency, except for pKC199βgeo, reported by Thomas *et al.* (2000). The vector pKC199βgeo also has an in-frame stop codon with the ATG of the *βgeo*, although they did not describe it but discussed other four possible reasons for the tendency to integrate into the 5′-end of genes. Thus, the structure of the SA carrying in-frame stop codon with the start codon of the *βgeo* would be useful for enriching integration near the 5′ end of genes.

In 64% of the trap clones, pU-17 vector was integrated into the downstream of the exon containing the start codon of the trapped gene (Fig. 2B). It is known that upstream AUG codons and open reading frames (uAUG/uORF) are common features of mRNA for mainly negative control of translation from the main AUG (Morris & Geballe 2000; Kozak 2002), and it is estimated that about half of human mRNA have uAUG/uORF (Suzuki *et al.* 2000). Leaky scanning and reinitiation mechanisms of ribosomes enable the downstream main AUG codons to be accessed by translation machinery (Kozak 2002). Although uAUG/uORF diminish translation of the main ORF, it is reported that approximately 40% of ribosomes were able to initiate twice and approximately 25% were able to initiate three times (Wang & Rothnagel 2004). Because the ORF started from endogenous AUG should act as uORF in 'downstream-integrated' trap clones, it is considered that the translation initiation of the *βgeo* would be somewhat lower level than that of the endogenous trapped gene, but enough for acquirement of G418 resistance. Whether the βgal activity in 'downstream-integrated' trap mice exactly reflect the expression pattern of the trapped genes or not can be easily tested by targeted insertion of the IRES-LacZ construct, and this analysis is now in progress.

We have performed targeted integration with more than 20 exchangeable trap clones, and in all clones except for one (Araki *et al.* 1999), we successfully obtained recombined clones at high frequencies of 80–95%. Thus, the targeted integration is highly reproducible. Our exchangeable gene trap system can overcome the limitations of conventional gene trapping and will be an ideal means for large-scale mutagenesis.

Acknowledgements

We wish to thank Ms Y. Mine, Y. Tsuruta, I. Kawasaki and M. Nakata for their technical assistance. This study was supported in part by a Grant-in-Aid on Priority Areas from the Ministry of Education, Science, Culture and Sports of Japan and a grant from the Osaka Foundation of Promotion of Clinical Immunology.

References

Albert, H., Dale, E. C., Lee, E. & Ow, D. W. 1995. Site-specific integration of DNA into wild-type and mutant *lox* sites placed in the plant genome. *Plant J.* **7**, 649–659.

Altschul, S. F., Gish, W., Miller, W., Myers, E. W. & Lipman, D. J. 1990. Basic local alignment search tool. *J. Mol. Biol.* **215**, 403–410.

Araki, K., Araki, M., Miyazaki, J. & Vassalli, P. 1995. Site-specific recombination of a transgene in fertilized eggs by transient expression of Cre recombinase. *Proc. Natl Acad. Sci. USA* **92**, 160–164.

Araki, K., Araki, M. & Yamamura, K. 1997. Targeted integration of DNA using mutant lox sites in embryonic stem cells. *Nucleic Acids Res.* **25**, 868–872.

Araki, K., Araki, M. & Yamamura, K. 2002. Site-directed integration of the cre gene mediated by Cre recombinase using a combination of mutant *lox* sites. *Nucleic Acids Res.* **30**, e103.

Araki, K., Imaizumi, T., Okuyama, K., Oike, Y. & Yamamura, K. 1997. Efficiency of recombination by Cre transient expression in embryonic stem cells: comparison of various promoters. *J. Biochem. (Tokyo)* **122**, 977–982.

Araki, K., Imaizumi, T., Sekimoto, T. *et al.* 1999. Exchangeable gene trap using the Cre/mutated *lox* system. *Cell Mol. Biol. (Noisy-le-Grand)* **45**, 737–750.

Bonaldo, P., Chowdhury, K., Stoykova, A., Torres, M. & Gruss, P. 1998. Efficient gene trap screening for novel developmental genes using IRES βgeo vector and in vitro preselection. *Exp. Cell Res.* **244**, 125–136.

Chowdhury, K., Bonaldo, P., Torres, M., Stoykova, A. & Gruss, P. 1997. Evidence for the stochastic integration of gene trap vectors into the mouse germline. *Nucleic Acids Res.* **25**, 1531–1536.

Evans, M. J., Carlton, M. B. L. & Russ, A. P. 1997. Gene trapping and functional genomics. *Trends Genet* **13**, 370–374.

Friedrich, G. & Soriano, P. 1991. Promoter traps in embryonic stem cells: a genetic screen to identify and mutate developmental genes in mice. *Genes Dev.* **5**, 1513–1523.

Ghattas, I. R., Sanes, J. R. & Majors, J. E. 1991. The encephalomyocarditis virus internal ribosome entry site allows efficient coexpression of two genes from a recombinant provirus in cultured cells and in embryos. *Mol. Cell Biol.* **11**, 5848–5859.

Gossler, A. & Zachgo, J. 1993. Gene and enhancer trap screens in ES cell chimeras. *Gene Targeting: a Practical Approach.* (ed. Joyner A.) pp. 181–227. Oxford University Press, Oxford.

Gossler, A., Joyner, A. L., Rossant, J. & Skarnes, W. C. 1989. Mouse embryonic stem cells and reporter constructs to detect developmentally regulated genes. *Science* **244**, 463–465.

Hansen, J., Floss, T., Van Sloun, P. *et al.* 2003. A large-scale, gene-driven mutagenesis approach for the functional analysis of the mouse genome. *Proc. Natl Acad. Sci. USA* **100**, 9918–9922.

Hildebrand, J. D. & Soriano, P. 1999. Shroom, a PDZ. domain-containing actin-binding protein, is required for neural tube morphogenesis in mice. *Cell* **99**, 485–497.

Jang, S. K. & Wimmer, E. 1990. Cap-independent translation of encephalomyocarditis virus RNA: structural elements of the internal ribosomal entry site and involvement of a cellular 57-kD RNA-binding protein. *Genes Dev.* **4**, 1560–1572.

Kang, H. M., Kang, N. G., Kim, D. G. & Shin, H. S. 1997. Dicistronic tagging of genes active in embryonic stem cells of mice. *Mol. Cells* **7**, 502–508.

Kozak, M. 2002. Pushing the limits of the scanning mechanism for initiation of translation. *Gene* **299**, 1–34.

von Melchner, H., DeGregori, J. V., Rayburn, H., Reddy, S., Friedel, C. & Ruley, H. E. 1992. Selective disruption of genes expressed in totipotent embryonal stem cells. *Genes Dev.* **6**, 919–927.

Morris, D. R. & Geballe, A. P. 2000. Upstream open reading frames as regulators of mRNA translation. *Mol. Cell Biol.* **20**, 8635–8642.

Mountford, P. S. & Smith, A. G. 1995. Internal ribosome entry sites and dicistronic RNAs in mammalian transgenesis. *Trends Genet* **11**, 179–184.

Niwa, H., Masui, S., Chambers, I., Smith, A. G. & Miyazaki, J. 2002. Phenotypic complementation establishes requirements for specific POU domain and generic transactivation function of Oct – 3/4 in embryonic stem cells. *Mol. Cell Biol.* **22**, 1526–1536.

Oike, Y., Hata, A., Mamiya, T. *et al.* 1999. Truncated CBP protein leads to classical Rubinstein–Taybi syndrome phenotypes in mice: implications for a dominant-negative mechanism. *Hum. Mol. Genet* **8**, 387–396.

Ringrose, L., Lounnas, V., Ehrlich, L. *et al.* 1998. Comparative kinetic analysis of FLP and cre recombinases: mathematical models for DNA binding and recombination. *J. Mol. Biol.* **284**, 363–384.

Stanford, W. L., Cohn, J. B. & Cordes, S. P. 2001. Gene-trap mutagenesis: past, present and beyond. *Nat. Rev. Genet* **2**, 756–768.

Stoykova, A., Chowdhury, K., Bonaldo, P. *et al.* 1998. Gene trap expression and mutational analysis for genes involved in the development of the mammalian nervous system. *Dev. Dyn.* **212**, 198–213.

Stryke, D., Kawamoto, M., Huang, C. C. *et al.* 2003. BayGenomics: a resource of insertional mutations in mouse embryonic stem cells. *Nucleic Acids Res.* **31**, 278–281.

Suzuki, Y., Ishihara, D., Sasaki, M. *et al.* 2000. Statistical analysis of the 5′ untranslated region of human mRNA using 'Oligo-Capped' cDNA libraries. *Genomics* **64**, 286–297.

Thomas, T., Voss, A. K., Chowdhury, K. & Gruss, P. 2000. A new gene trap construct enriching for insertion events near the 5′ end of genes. *Transgenic Res.* **9**, 395–404.

Townley, D. J., Avery, B. J., Rosen, B. & Skarnes, W. C. 1997. Rapid sequence analysis of gene trap integrations to generate a resource of insertional mutations in mice. *Genome Res.* **7**, 293–298.

Voss, A. K., Thomas, T. & Gruss, P. 1998. Efficiency assessment of the gene trap approach. *Dev. Dyn.* **212**, 171–180.

Wagner, E. & Lykke-Andersen, J. 2002. mRNA surveillance: the perfect persist. *J. Cell Sci.* **115**, 3033–3038.

Wang, X. Q. & Rothnagel, J. A. 2004. 5′-untranslated regions with multiple upstream AUG codons can support low-level translation via leaky scanning and reinitiation. *Nucleic Acids Res.* **32**, 1382–1391.

Waterston, R. H., Lindblad-Toh, K., Birney, E. *et al.* 2002. Initial sequencing and comparative analysis of the mouse genome. *Nature* **420**, 520–562.

Yagi, T., Tokunaga, T., Furuta, Y. *et al.* 1993. A novel ES cell line, TT2, with high germline-differentiating potency. *Anal Biochem.* **214**, 70–76.

Yamamura, K., Kikutani, H., Takahashi, N. *et al.* 1984. Introduction of human γ1 immunoglobulin genes into fertilized mouse eggs. *J. Biochem. (Tokyo)* **96**, 357–363.

Zambrowicz, B. P. & Friedrich, G. A. 1998. Comprehensive mammalian genetics: history and future prospects of gene trapping in the mouse. *Int. J. Dev. Biol.* **42**, 1025–1036.

nature medicine

Angiopoietin-related growth factor antagonizes obesity and insulin resistance

Yuichi Oike[1], Masaki Akao[1], Kunio Yasunaga[2], Toshimasa Yamauchi[3], Tohru Morisada[1], Yasuhiro Ito[1], Takashi Urano[1], Yoshishige Kimura[1], Yoshiaki Kubota[1], Hiromitsu Maekawa[1], Takeshi Miyamoto[1], Keishi Miyata[1], Shun-ichiro Matsumoto[2], Juro Sakai[4], Naomi Nakagata[5], Motohiro Takeya[6], Haruhiko Koseki[7], Yoshihiro Ogawa[8], Takashi Kadowaki[3] & Toshio Suda[1]

Angiopoietin-related growth factor (AGF), a member of the angiopoietin-like protein (Angptl) family, is secreted predominantly from the liver into the systemic circulation. Here, we show that most (>80%) of the AGF-deficient mice die at about embryonic day 13, whereas the surviving AGF-deficient mice develop marked obesity, lipid accumulation in skeletal muscle and liver, and insulin resistance accompanied by reduced energy expenditure relative to controls. In parallel, mice with targeted activation of AGF show leanness and increased insulin sensitivity resulting from increased energy expenditure. They are also protected from high-fat diet–induced obesity, insulin resistance and nonadipose tissue steatosis. Hepatic overexpression of AGF by adenoviral transduction, which leads to an approximately 2.5-fold increase in serum AGF concentrations, results in a significant ($P < 0.01$) body weight loss and increases insulin sensitivity in mice fed a high-fat diet. This study establishes AGF as a new hepatocyte-derived circulating factor that counteracts obesity and related insulin resistance.

Obesity is an increasingly prevalent medical and social problem with potentially devastating consequences because it clusters with type 2 diabetes, hypertension and hyperlipidemia in the metabolic syndrome or syndrome X[1,2]. The molecular mechanisms underlying obesity have not been fully clarified, and effective therapeutic approaches are currently of general interest. Inhibition of weight gain requires that we burn more calories than we take in. From this perspective, adaptive thermogenesis, which is the process of heat production in response to diet or environment temperature, is an important defense against obesity[3,4].

Recently, we and several groups independently identified several molecules containing a coiled-coil domain and a fibrinogen-like domain, motifs structurally conserved in angiopoietins[5,6]. Because these molecules do not bind the angiopoietin receptor, Tie-2, they were named angiopoietin-like proteins (Angptl). We identified angiopoietin-related growth factor (AGF, also known as Angptl6 and encoded by the gene *Angptl6*) as a member of the Angptl family and showed that it is a circulating orphan peptide secreted by liver that induces angiogenesis and proliferation of skin cells, and thereby promotes wound healing[6–8]. Furthermore, several early reports have indicated that there are additional members of the Angptl family, which are currently considered orphan ligands, as angiogenic factors in the vascular system[6,9–11]. On the other hand, several reports indicate that Angptls have biological effects on nonvascular cells. For example, Angptl4 (refs. 12,13; also known as PGAR and FIAF) and Angptl3 (refs. 14,15) regulate fat and/or lipid metabolic homeostasis in addition to controlling angiogenesis[10,11]. These findings suggest that Angptls exert multiple biological functions; however, the physiological and pathological roles of each member of the Angptls have not been fully clarified.

Here we show that most (>80%) of the mice with mutations in AGF (*Angptl6*$^{-/-}$ mice) die at about embryonic day 13, with apparent cardiovascular defects including poorly formed yolk sac and vitelline vessels. Notably, the surviving *Angptl6*$^{-/-}$ mice become markedly obese and have obesity-related metabolic disorders. In parallel, mice with targeted activation of AGF *in vivo* (*Angptl6*-transgenic mice) show markedly reduced adiposity and insulin sensitivity. Furthermore, *Angptl6*-transgenic mice are completely resistant to high-fat diet–induced obesity and impaired insulin sensitivity. Moreover, we found that hepatic overexpression of AGF by adenoviral transduction, which leads to an approximately 2.5-fold increase in serum AGF concentrations, results in a significant ($P < 0.01$) body weight loss and ameliorates insulin sensitivity in mice fed a high-fat diet. Based on these findings, we report here that AGF is a new hepatocyte-derived circulating factor counteracting high-fat diet–induced obesity and related insulin resistance through increased energy expenditure, thereby suggesting a therapeutic potential in counteracting obesity and diabetes.

[1]Department of Cell Differentiation, The Sakaguchi Laboratory, School of Medicine, Keio University, 35 Shinanomachi, Shinjuku-ku, Tokyo 160-8582, Japan. [2]Molecular Medicine Laboratories, Yamanouchi Pharmaceutical Co., Ltd., Tsukuba, 305-8585, Japan. [3]Department of Internal Medicine, Graduate School of Medicine, University of Tokyo, Tokyo 113-8655, Japan. [4]Research Center for Advanced Science and Technology, University of Tokyo, Tokyo 153-8904, Japan. [5]Center for Animal Resources and Development, and [6]Department of Pathology, Kumamoto University, Kumamoto 860-0811, Japan. [7]RIKEN Research Center for Allergy and Immunology, Tsurumi-ku, Yokohama 230-0045, Japan. [8]Department of Molecular Medicine and Metabolism, Medical Research Institute, Tokyo Medical and Dental University, Tokyo 101-0062, Japan. Correspondence should be addressed to Y.O. (oike@sc.itc.keio.ac.jp).

Published online 20 March 2005; doi:10.1038/nm1214

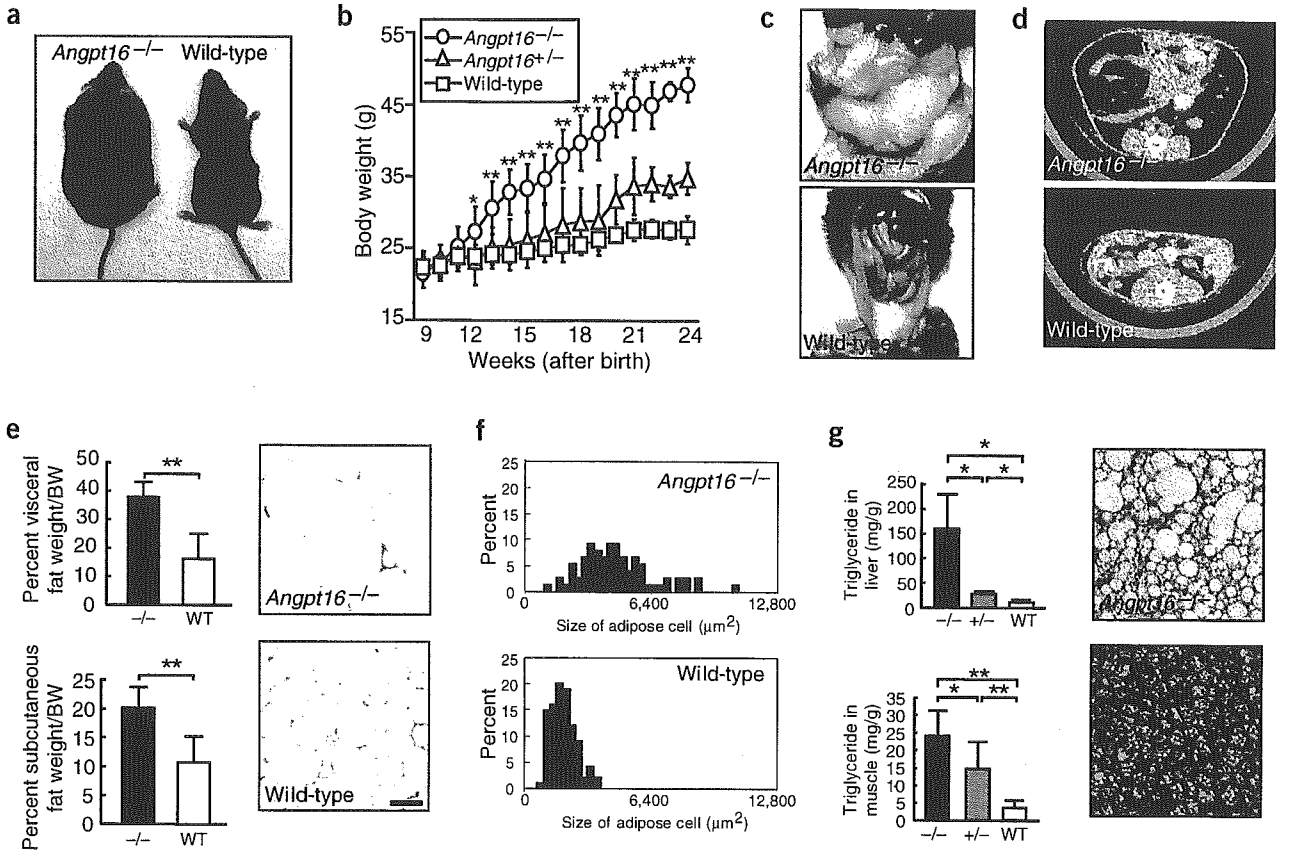

Figure 1 Obesity in *Angptl6*$^{-/-}$ mice on a normal diet. (**a**) Gross appearance of *Angptl6*$^{-/-}$ mice and wild-type control mice. (**b**) Body weight of each genotype ($n = 8$). (**c–g**) Abdominal cavity (**c**), CT findings at a level of 8 mm above the top of the iliac bone (**d**), visceral fat ($n = 5$) and subcutaneous fat ($n = 5$) weight/body weight, and histological analysis (**e**) and distribution of cell size (**f**) of WAT of *Angptl6*$^{-/-}$ mice and wild-type mice. (**g**) Triglyceride levels in liver ($n = 5$) and gastrocnemius muscle ($n = 5$), and hematoxylin and eosin–stained sections of BAT of *Angptl6*$^{-/-}$ and wild-type mice. Data are mean ± s.d. Bars in histological sections indicate 50 μm. $^*P < 0.05$, $^{**}P < 0.01$, between the two genotypes indicated. Female mice 8 months after birth were used for all experiments.

RESULTS

Disruption of *Angptl6 in vivo*

To investigate the physiological role of AGF, we generated mice with mutations in *Angptl6* (**Supplementary Fig. 1** online). Most (>80%) of *Angptl6*$^{-/-}$ mice die at approximately embryonic day 13 (**Supplementary Fig. 1**), with apparent cardiovascular defects including poorly formed yolk sac and vitelline vessels (data not shown). Notably, the surviving *Angptl6*$^{-/-}$ mice become markedly obese even on a normal chow diet, suggesting that AGF has a crucial role in regulating adiposity in adulthood (**Fig. 1a**). We therefore focused on how AGF functions in the pathogenesis of obesity and associated disorders.

Obesity in *Angptl6*$^{-/-}$ mice

Twelve weeks after birth, *Angptl6*$^{-/-}$ mice showed increases in body weight that surpassed those seen in wild-type (*Angptl6*$^{+/+}$) mice on a normal chow diet (**Fig. 1b**). There were no phenotypic differences between male and female mice. Macroscopic and computed tomographic (CT) analyses taken 8 months after birth showed that both visceral and subcutaneous fat depots were significantly increased in *Angptl6*$^{-/-}$ mice compared to wild-type mice (**Fig. 1c–e**). Sections of white adipose tissue (WAT) from *Angptl6*$^{-/-}$ mice showed increased adipocyte size relative to controls (**Fig. 1e,f**). A large amount of lipid accumulation in liver, skeletal muscle and brown adipose tissue (BAT) was observed in *Angptl6*$^{-/-}$ mice compared with *Angptl6*$^{+/-}$ and wild-type mice (**Fig. 1g**).

Metabolic disorders in *Angptl6*$^{-/-}$ mice

To address alternative causes of increased body weight in *Angptl6*$^{-/-}$ mice, we compared lipid metabolism, rectal temperature, basal metabolic rate and food intake of *Angptl6*$^{-/-}$ and wild-type mice. Significant increases were observed in serum cholesterol and free fatty acid (FFA) concentrations in *Angptl6*$^{-/-}$ mice, whereas there were no significant differences in serum triglyceride concentration between genotypes (**Fig. 2a**). *Angptl6*$^{-/-}$ mice also showed significant decreases in rectal temperature and whole-body oxygen consumption rates compared with wild-type mice (**Fig. 2b**). A small, statistically insignificant increase was observed in daily food intake in *Angptl6*$^{-/-}$ mice compared with controls (**Fig. 2b**).

Adipose tissue has a substantial influence on systemic glucose homeostasis through secretion of adipocytokines[2,16,17]. *Angptl6*$^{-/-}$ mice showed mild hyperglycemia and severe hyperinsulinemia (**Fig. 2c**). To investigate this point further, we performed intraperitoneal glucose and insulin tolerance tests (IGTT and IITT, respectively). Both hyperglycemia and hyperinsulinemia were detected in *Angptl6*$^{-/-}$ mice throughout the time course of the experiment

(Fig. 2c). Moreover, the glucose-lowering effect of insulin was decreased in *Angptl6*$^{-/-}$ mice relative to controls, indicating insulin resistance in *Angptl6*$^{-/-}$ mice (**Fig. 2d**). Recent studies have shown a role for tumor necrosis factor (TNF)-α[18,19] secreted from adipose tissue as a mediator of insulin resistance, and adiponectin[20,21] and leptin[22,23] have a role in insulin sensitivity. The leptin concentration in *Angptl6*$^{-/-}$ mice was significantly higher than that seen in controls, whereas no significant differences were observed in adiponectin and TNF-α concentrations between genotypes (**Fig. 2e**).

Molecular alterations in *Angptl6*$^{-/-}$ mice

The physiological data presented above indicate that inactivation of AGF *in vivo* leads to decreased energy expenditure and obesity. Recent studies indicate that BAT and skeletal muscle function as tissues mediating adaptive thermogenesis, which is an important defense against obesity[24,25]. To determine the molecular basis of these metabolic changes in *Angptl6*$^{-/-}$ mice, we examined the expression of molecules with proposed roles in obesity and associated metabolic action in BAT and skeletal muscle. Quantitative RT-PCR analysis showed significant decreases in expression of PPARα, PPARγ, PGC-1β and UCP1 in BAT (**Fig. 2f**) and PPARδ and UCP3 in skeletal muscle (**Fig. 2g**) in *Angptl6*$^{-/-}$ mice, suggesting that such alterations in gene expression underlie susceptibility to obesity in *Angptl6*$^{-/-}$ mice.

Generation of *Angptl6*-transgenic mice

Observations that AGF ablation causes obesity prompted us to further investigate whether AGF functions in resistance to obesity and associated disorders. To generate mice overexpressing AGF constitutively, we targeted the activation of *Angptl6 in vivo* by driving its expression from the chicken β-actin promoter with the cytomegalovirus immediate-early enhancer (CAG promoter)[26,27] (**Supplementary Fig. 2** online). The CAG promoter has been reported to be strongly active in a variety of tissues. In our mice, the promoter drove high expression of the *Angptl6* transgene in BAT, heart and skeletal muscle relative to expression of the endogenous gene in each tissue (**Supplementary Fig. 2**). AGF concentration in the circulation of *Angptl6* transgenic mice increased approximately twofold compared with basal concentrations in nontransgenic controls (**Fig. 3a**).

Leanness in *Angptl6* transgenic mice

Despite a daily food intake similar to that of controls when individually housed and fed a normal chow diet (transgenic mice, 0.17 ± 0.05

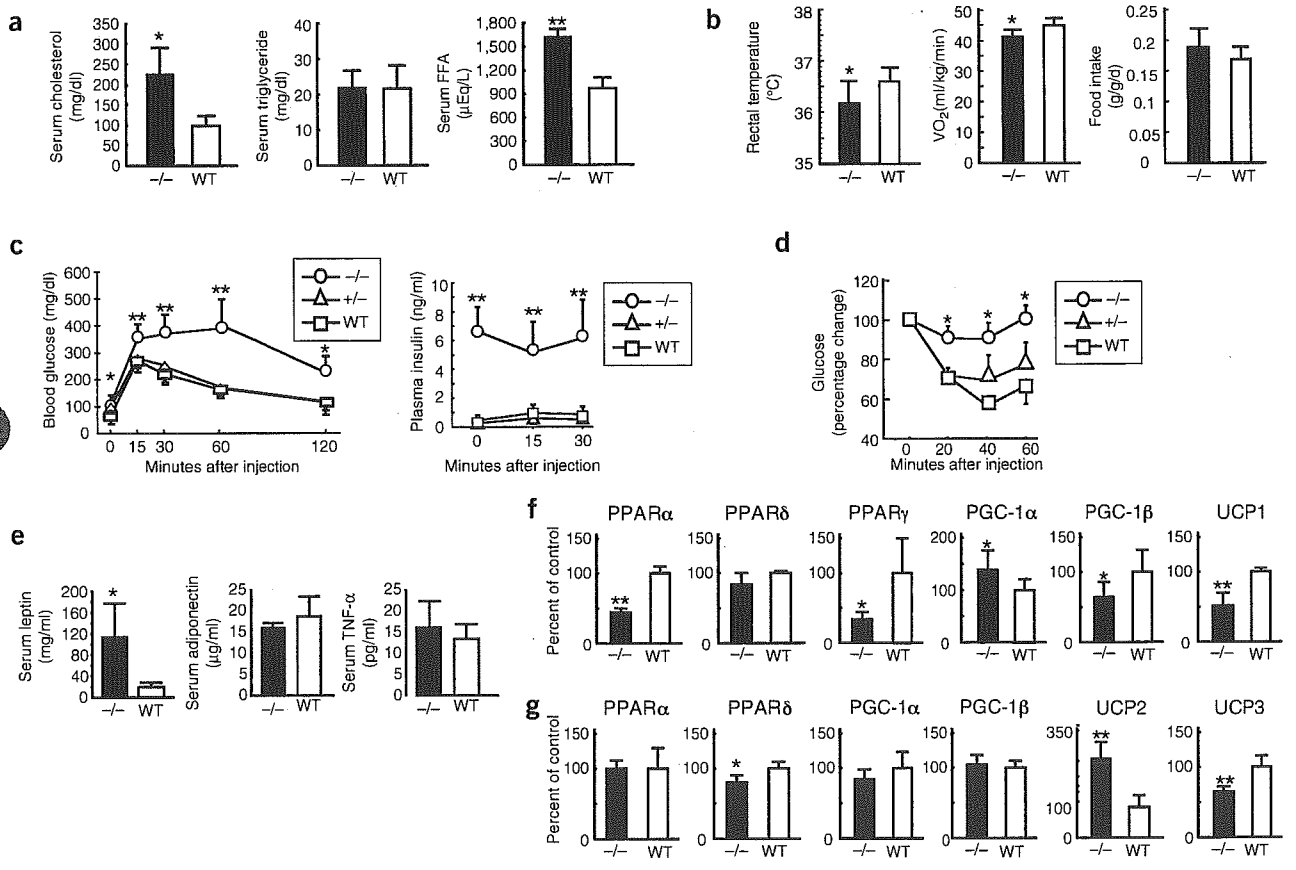

Figure 2 Metabolic effects of AGF deficiency on a normal diet. (**a**) Serum cholesterol, triglyceride and FFA concentrations in *Angptl6*$^{-/-}$ and wild-type control mice at 5 months of age ($n = 5$ in each group). (**b**) Rectal temperature, oxygen consumption (VO_2)/lean body weight and food intake/lean body weight in *Angptl6*$^{-/-}$ and wild-type mice at 6 months of age ($n = 8$ in each group). (**c**,**d**) Glucose (**c**) and insulin (**d**) tolerance tests in *Angptl6*$^{-/-}$, *Angptl6*$^{+/-}$ and wild-type mice at 3 months of age ($n = 6$ in each group). (**e**) Serum leptin, adiponectin, and TNF-α concentrations in *Angptl6*$^{-/-}$ and wild-type mice at 5 months of age ($n = 5$ in each group). (**f**,**g**) Expression of genes associated with energy expenditure in BAT (**f**) and skeletal muscle (**g**) of *Angptl6*$^{-/-}$ relative to wild-type mice (100%) at 3 months of age ($n = 5$ in each group). Data are mean ± s.d. $^*P < 0.05$, $^{**}P < 0.01$, between the two genotypes indicated or among three genotypes. Female mice were used for all experiments.

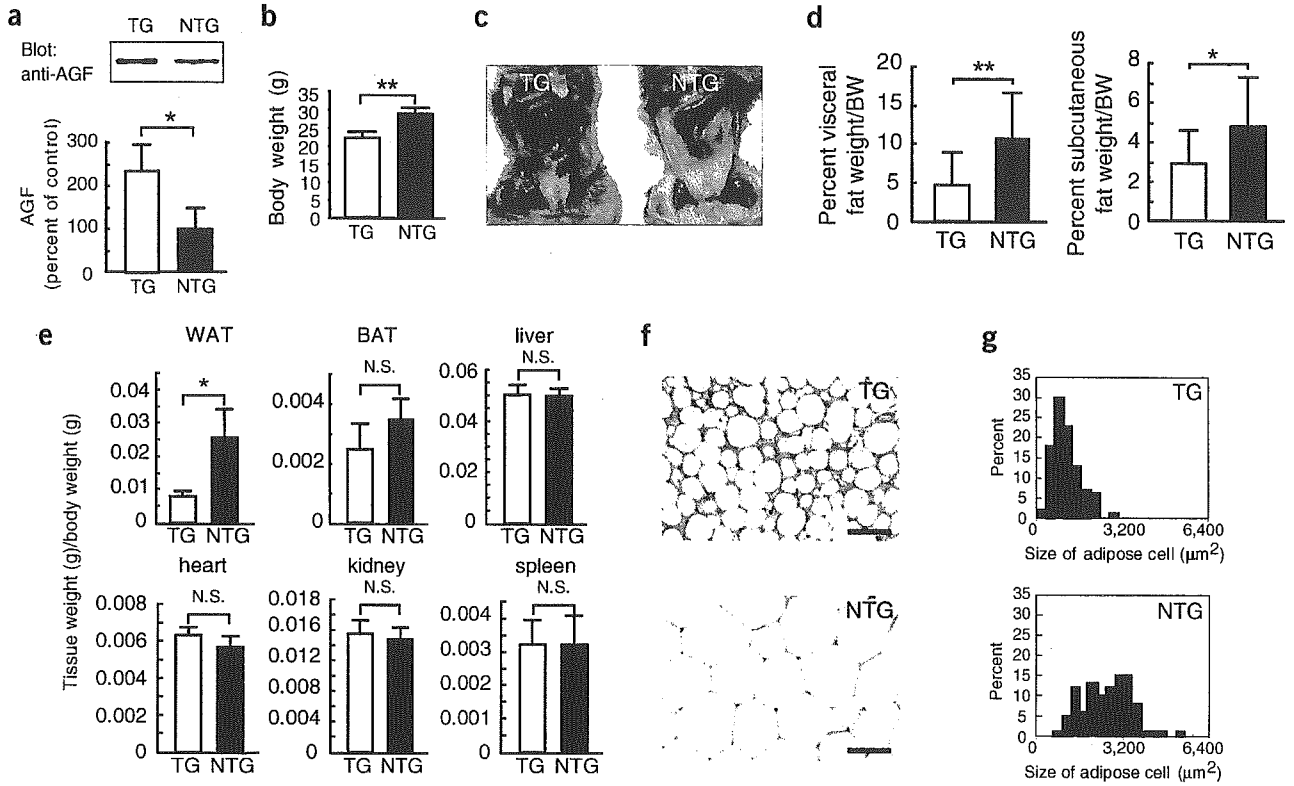

Figure 3 *Angptl6* transgenic mice are lean as a result of a loss of WAT mass. (**a**) Western blotting analysis for serum AGF in *Angptl6* transgenic (TG) and nontransgenic control (NTG) mice at 4 months of age. The ratio for the control is set as 100%. (**b–g**) Body weight (**b**), and gross appearance of visceral adipocyte (**c**) in TG and NTG mice at 4 months of age. (**d**) Comparison of visceral fat and subcutaneous fat weight/body weight between TG and NTG mice at 5 months of age. Tissue weight/body weight in TG and NTG mice at 4 months of age (**e**). $n = 10–15$ in each group. Histological analysis (**f**) and distribution of cell size (**g**) of WAT from TG and NTG mice at 4 months of age. Scale bars, 50 μm. Data are mean ± s.d. $^*P < 0.05$, $^{**}P < 0.01$, between the two genotypes indicated. N.S. indicates no significant difference compared with nontransgenic wild-type mice. Female mice were used for all experiments.

versus control mice, 0.15 ± 0.03 g/g lean body mass/d), 5-month-old *Angptl6* transgenic mice showed marked reductions in body weight and adiposity compared with controls (**Fig. 3b–d**). Although there was no alteration in body weight at birth between genotypes, a reduction in body weight of *Angptl6* transgenic mice compared to controls was noted 4 weeks after birth and persisted throughout their life. There were no differences of this alteration in body weight between male and female mice. Furthermore, only WAT weight per body weight in *Angptl6* transgenic mice was markedly decreased compared to that of controls (**Fig. 3e**). Adipocytes from *Angptl6* transgenic mice are smaller in size compared to those from controls, indicating that a reduction in total fat mass may result from decreased triglyceride accumulation (**Fig. 3f,g**).

Metabolic alterations in *Angptl6* transgenic mice

There was no difference in *in vitro* adipocyte differentiation of embryonic fibroblasts between *Angptl6* transgenic mice and controls (data not shown). To address alternative causes for decreased adiposity in *Angptl6* transgenic mice, we compared rectal temperature and basal metabolic rates of *Angptl6* transgenic mice and controls. Transgenic mice showed a small, statistically insignificant increase in rectal temperature and a statistically significant increase in whole-body oxygen consumption rates relative to controls (**Fig. 4a**), suggesting the enhanced energy expenditure in *Angptl6* transgenic mice. The microvasculature assists in heat dissipation at sites of active thermogenesis, increasing the efficiency of lipid release from fat stores[28,29]. *Angptl6* transgenic mice showed an increase in the number of capillary-sized vessels in skeletal muscles compared to controls (**Fig. 4b**), suggesting that AGF assists in part to increase thermogenesis in *Angptl6* transgenic mice.

Quantitative RT-PCR analysis showed significant increases in expression of the genes encoding PPARα, PPARγ and PGC-1β in BAT (**Fig. 4c**) and of the genes encoding PPARα, PPARδ, PGC-1α and UCP2 in skeletal muscle (**Fig. 4d**) in *Angptl6* transgenic mice. These findings suggest that overexpression of AGF *in vivo* activates molecules involved in stimulating energy expenditure, and thereby leads to decreased adiposity.

Insulin sensitivity in *Angptl6* transgenic mice

A lack of fat causes decreases in serum levels of leptin and adiponectin and leads to insulin resistance and diabetes[21,22,30,31]. Although *Angptl6* transgenic mice showed decreased serum leptin levels, identical serum adiponectin levels were observed in transgenic and wild-type mice (**Fig. 4e**). Serum adiponectin levels per WAT mass in *Angptl6* transgenic mice were markedly increased compared with that of wild-type mice, whereas there was no difference in serum leptin levels per WAT mass (**Fig. 4e**), suggesting that adipose tissues in *Angptl6* transgenic mice secrete adiponectin abundantly. Notably, IGTT and IITT showed that *Angptl6* transgenic mice show increased insulin sensitivity despite the greatly decreased serum leptin and identical serum adiponectin levels

(Fig. 4f,g), suggesting that increased insulin sensitivity observed in *Angptl6* transgenic mice depends on direct effects of increased serum AGF.

Resistance to obesity in *Angptl6*-transgenic mice

To investigate whether *Angptl6* transgenic mice show resistance against developing obesity, we challenged 8-week-old female mice with a high-fat diet containing 32% (wt/wt) fat for 12 weeks to stimulate weight gain. *Angptl6* transgenic mice fed this diet showed significant differences from controls: at the end of the feeding period, the net weight gains were 7.13 ± 1.03 g and 21.86 ± 4.03 g, respectively, for *Angptl6* transgenic and controls (**Fig. 5a,b**). As expected, high-fat feeding causes massive lipid accumulation in both visceral and subcutaneous fat depots in controls, whereas few of these changes are seen in *Angptl6* transgenic mice (**Fig. 5c,d**). Notably, the size of WAT from *Angptl6* transgenic mice was markedly smaller than that of WAT from controls (**Fig. 5e**). No appreciable fatty acid accumulation in BAT, liver and skeletal muscle was observed in *Angptl6* transgenic mice, whereas nontransgenic mice develop tissue steatosis (**Fig. 5e,f**). There was no significant difference in blood glucose levels between genotypes (**Fig. 5g**). But plasma insulin levels in *Angptl6* transgenic mice were much lower than those seen in controls (**Fig. 5g**). Whereas high-fat feeding increases serum cholesterol and FFA levels by twofold in controls, *Angptl6* transgenic mice showed a lipid profile closer to that of wild-type mice fed a standard chow diet (**Fig. 5g**).

AGF antagonizes obesity and insulin resistance

To clarify whether AGF decreases body weight and insulin resistance of obese mice, we intravenously injected adenovirus expressing mouse AGF (Ad-AGF) into female mice fed a high-fat diet containing 32% (wt/wt) fat for 12 months. For controls, adenovirus expressing green fluorescent protein (GFP) (Ad-GFP) was injected. There was no significant difference in body weight between the mice with AGF treatment and controls (54.4 ± 2.2 g and 52.9 ± 2.1 g, respectively: $P = 0.18$, $n = 8$). Throughout the time course of the experiment, mice continued to receive a high-fat diet. On day 20, mice receiving AGF showed approximately 2.5-fold increases in serum AGF levels compared to controls (**Fig. 6a**), and showed significant loss of body weight compared to controls (**Fig. 6b**). No significant difference between the two groups was observed in daily food intake (**Fig. 6c**). Furthermore, significant decreases in fasting and random fed glucose levels were observed in high-fat diet–induced obese mice after treatment with AGF compared to those in controls (**Fig. 6d,e**). IGTT and IITT showed that high-fat diet–induced obese mice with AGF treatment showed improved glucose tolerance and increased insulin sensitivity (**Fig. 6f,g**). Taken together, these data clearly show that AGF counteracts obesity and related insulin resistance.

DISCUSSION

AGF, a member of the Angptl family, is a circulating angiogenic protein secreted by liver[7]. Here, we show that most (>80%) of the AGF-deficient mice die at approximately embryonic day 13, with apparent cardiovascular defects including poorly formed yolk sac and vitelline vessels. Notably, the surviving *Angptl6*$^{-/-}$ mice become markedly obese and show obesity-related metabolic disorders. Furthermore, *Angptl6*$^{-/-}$ mice show decreased whole-body oxygen consumption and expression of genes involved in energy dissipation. In parallel, *Angptl6* transgenic mice show resistance against diet-induced obesity, insulin resistance and hyperlipidemia. These phenotypes are associated with increases in energy expenditure, supporting the hypothesis that AGF regulates energy metabolism in mice.

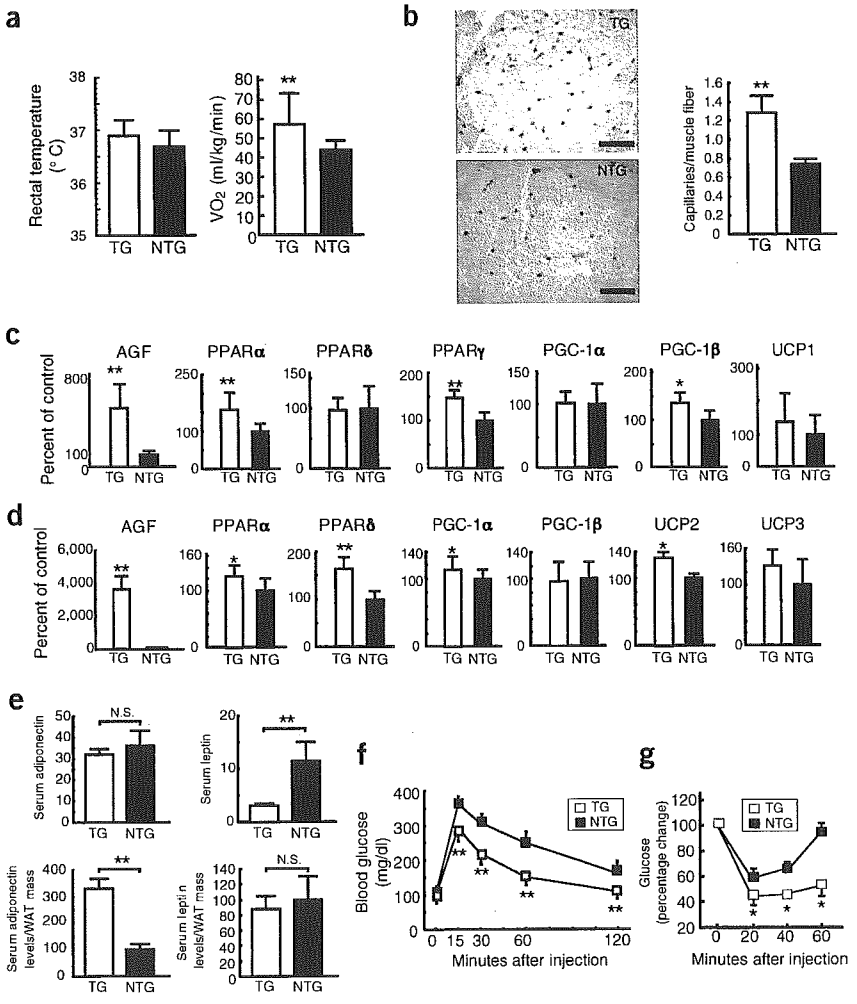

Figure 4 Metabolic and vascular alteration in *Angptl6* transgenic mice. (**a**) Rectal temperature and oxygen consumption (VO_2)/lean body weight in *Angptl6* transgenic (TG) and nontransgenic (NTG) female mice at 5 months of age ($n = 10$–12 in each group; these mice were also used in **Fig. 4e,f**). (**b**) Representative photograph of CD31/PECAM-1-stained capillary vessels and quantitative estimation of capillary vessel density in the gastrocnemius muscle in TG and NTG female mice at 4 months of age. Scale bars, 50 μm. (**c,d**) Relative ratio of gene expression associated with increased energy expenditure in BAT (**c**) and skeletal muscle (**d**) in TG mice relative to that seen in NTG female and male mice at 4 months of age. The ratio for the data from NTG mice is set as 100%. (**e**) Serum adiponectin and leptin levels and serum adiponectin and leptin levels/ WAT mass in TG and NTG female mice at 4 months of age. (**f,g**) Glucose (**f**) and insulin (**g**) tolerance tests in TG and NTG female mice at 4 months of age. Data are mean ± s.d. ($n = 5$–15). $^*P < 0.05$, $^{**}P < 0.01$, between the two genotypes indicated. N.S. indicates no significant difference compared with NTG mice.

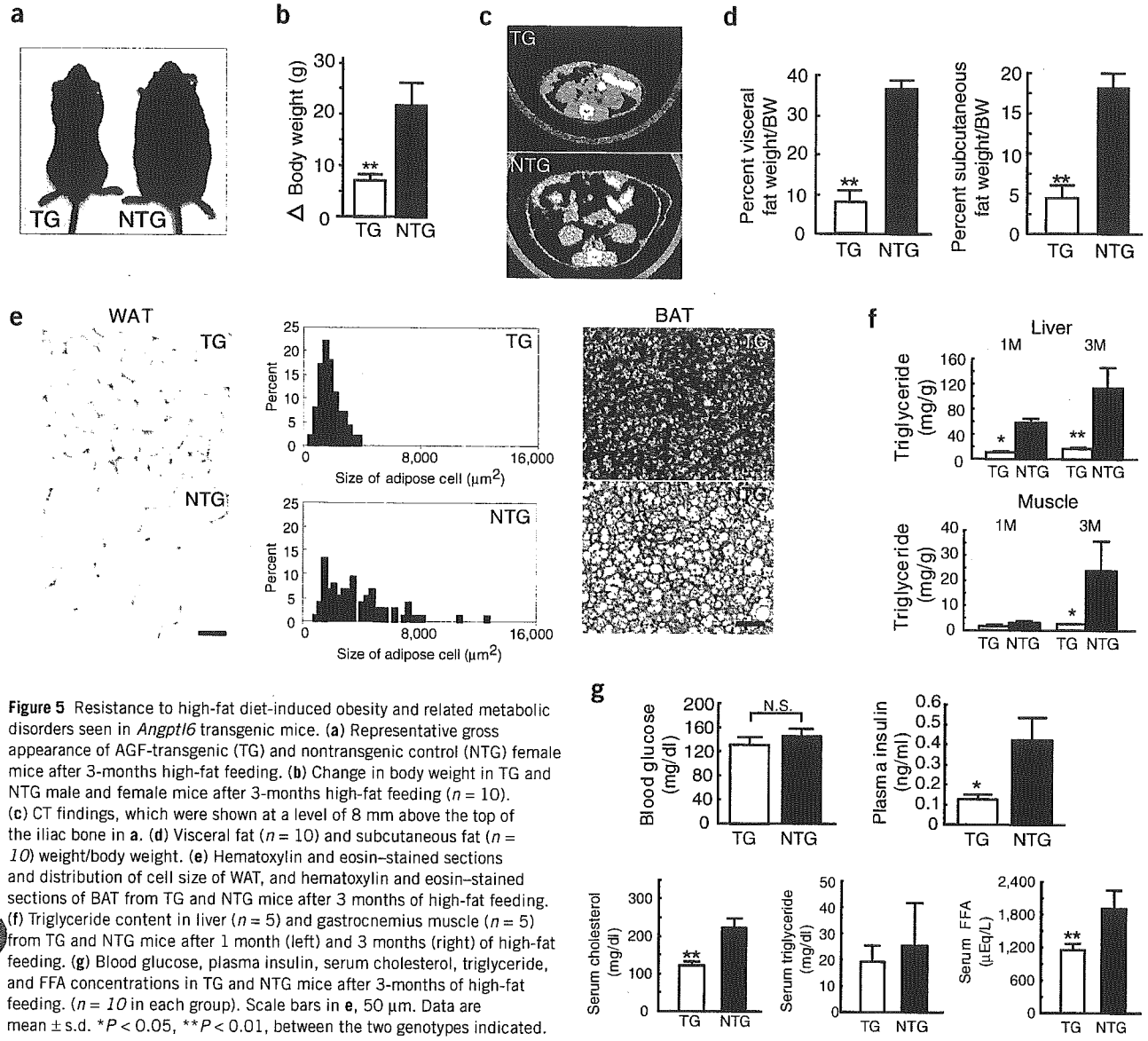

Figure 5 Resistance to high-fat diet-induced obesity and related metabolic disorders seen in *Angptl6* transgenic mice. (**a**) Representative gross appearance of AGF-transgenic (TG) and nontransgenic control (NTG) female mice after 3-months high-fat feeding. (**b**) Change in body weight in TG and NTG male and female mice after 3-months high-fat feeding ($n = 10$). (**c**) CT findings, which were shown at a level of 8 mm above the top of the iliac bone in **a**. (**d**) Visceral fat ($n = 10$) and subcutaneous fat ($n = 10$) weight/body weight. (**e**) Hematoxylin and eosin–stained sections and distribution of cell size of WAT, and hematoxylin and eosin–stained sections of BAT from TG and NTG mice after 3 months of high-fat feeding. (**f**) Triglyceride content in liver ($n = 5$) and gastrocnemius muscle ($n = 5$) from TG and NTG mice after 1 month (left) and 3 months (right) of high-fat feeding. (**g**) Blood glucose, plasma insulin, serum cholesterol, triglyceride, and FFA concentrations in TG and NTG mice after 3-months of high-fat feeding. ($n = 10$ in each group). Scale bars in **e**, 50 μm. Data are mean ± s.d. $^*P < 0.05$, $^{**}P < 0.01$, between the two genotypes indicated.

Metabolic analysis of energy balance using *Angptl6*$^{-/-}$ and *Angptl6* transgenic mice showed that one way AGF functions to regulate adiposity is through control of energy dissipation. Recent studies indicate that BAT and skeletal muscle regulate adaptive thermogenesis, which is mediated by PPARα, PPARδ, PPARγ and their coactivators, PGC-1α and PGC-1β, in response to energy overload[3,16,26,32–35]. We found statistically significant decreases in the expression of PPARα, PPARγ and PGC-1β in BAT and of PPARδ in skeletal muscle in *Angptl6*$^{-/-}$ mice, and increases in expression of PPARα, PPARγ and PGC-1β in BAT and of PPARα, PPARδ, and PGC-1α in skeletal muscle of *Angptl6* transgenic mice. In fact, *Angptl6* transgenic mice show phenotypes similar to those seen in transgenic mice with activated PPARδ[36–38] and PGC-1β[26]. Skeletal muscle is a direct target tissue of AGF, because AGF protein binds to C2C12 myocytes (**Supplementary Fig. 3** online). Treatment of C2C12 myocytes with AGF stimulated ligand activities of PPARα and PPARδ (**Supplementary Fig. 3**). Moreover, AGF activates p38 MAPK in muscle (**Supplementary Fig. 3**), which directly enhances the stabilization and activation of PGC-1 protein[34,35]. We therefore propose that AGF stimulates fat burning in peripheral tissues through the p38 MAPK pathway and downstream effects on respiration and gene expression linked to mitochondrial uncoupling and energy expenditure.

The microvasculature assists in heat dissipation at sites of active thermogenesis in peripheral tissues[28,29]. Because AGF increases the number of capillary-sized vessels in mice[8], we examined whether the vasculature is altered in *Angptl6*$^{-/-}$ and *Angptl6* transgenic mice. *Angptl6*$^{-/-}$ mice were susceptible to obesity and showed significantly ($P < 0.05$) decreased blood-flow perfusion in skeletal muscle, suggesting that loss of AGF enhances observed decreases in the efficiency in energy dissipation (**Supplementary Fig. 4** online). In parallel, a significant ($P < 0.01$) increase in the number of microvessels was observed in skeletal muscle of *Angptl6* transgenic mice, which may antagonize obesity by facilitat-

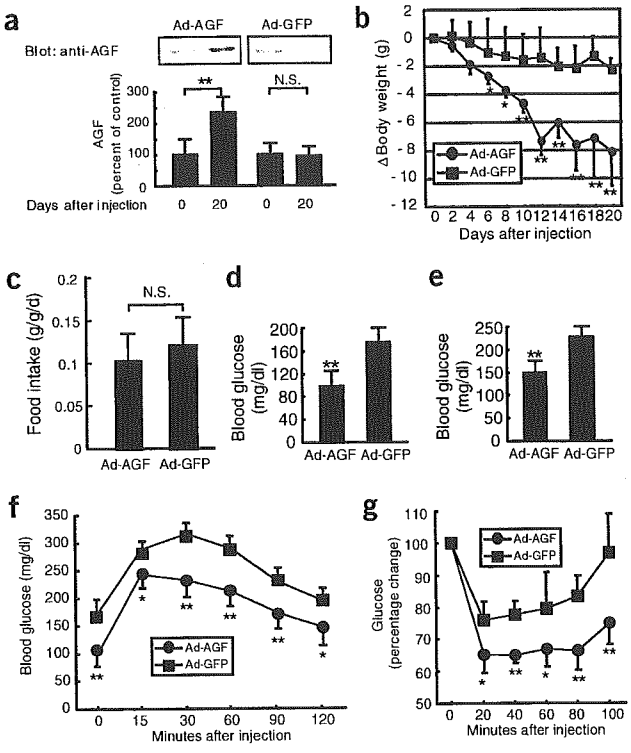

Figure 6 AGF decreased body weight and increased insulin sensitivity in high-fat fed-induced obese mice. (**a**) The relative ratio of serum concentrations of AGF in Ad-AGF injected and Ad-GFP injected mice on day 20 relative to each mouse on day 0. The value of serum AGF concentrations on day 0 is set at 100% (n = 5–8 in each group). (**b**) Alteration in body weight of high-fat fed-induced obese female mice after Ad-AGF and Ad-GFP injections (n = 8 in each group). (**c**–**g**) Comparison of food intake/lean body weight (**c**), fasting blood glucose (**d**), random fed blood glucose (**e**), glucose tolerance test (**f**) and insulin tolerance test (**g**) between Ad-AGF injected and Ad-GFP injected mice (n = 5-8 in each group). Data are mean ± s.d. $^*P < 0.05$, $^{**}P < 0.01$, between the two groups. N.S. indicates no significant difference compared with Ad-GFP–injected mice.

ing increases in energy dissipation. Furthermore, by providing a local angiogenic signal, AGF might increase the efficiency of lipid release from fat stores to maintain energy homeostasis. AGF induces angiogenesis in peripheral tissues, partially explaining how AGF counteracts obesity in addition to the direct effects of AGF on tissues functioning in adaptive thermogenesis.

Recent studies indicate that abnormal accumulation of triglycerides in muscle and liver results in insulin resistance by inhibiting insulin receptor signaling cascades[39,40]. Even on a high-fat diet, *Angptl6* transgenic mice are protected against hepatic and muscle steatosis, resulting in the maintenance of insulin sensitivity. These findings suggest that one mechanism whereby AGF affects insulin sensitivity is inhibition of abnormal lipid stores in insulin target tissues. Adipose tissue has a substantial impact on systemic glucose homeostasis through production of adipokines[34,35]. Recent studies show a role for adiponectin[20,21] and leptin[22,23] as mediators of insulin sensitivity and TNF-α[18,19] in mediating insulin resistance. In lipoatrophic diabetes, adiponectin and leptin deficiency resulting from lack of fat is associated with insulin resistance and diabetes[20,22,30,31]. Despite a greatly decreased WAT mass, *Angptl6* transgenic mice show increased insulin sensitivity, suggesting that AGF may increase insulin sensitivity. In contrast with decreased serum leptin levels, serum adiponectin levels in *Angptl6* transgenic mice were identical to those seen in wild-type mice. This may partially contribute to increased insulin sensitivity in *Angptl6* transgenic mice.

Findings derived from *Angptl6* transgenic mice, in which AGF expression is driven from the CAG promoter, led us to ask whether AGF in the circulation affects obesity and related metabolic abnormalities, because AGF is secreted primarily from hepatocytes. In this study, mice with high-fat diet–induced obesity overexpressing AGF in liver as a result of adenoviral transduction showed 2.5-fold increases in serum AGF levels over in controls and showed significant ($P < 0.01$) body weight loss and improved insulin sensitivity. Moreover, we observed that serum AGF levels in *Angptl6* transgenic mice described here and those seen in K14-*Angptl6* transgenic mice[7,8], in which AGF is driven by a skin-specific (K14) promoter, were approximately identical (**Supplementary Fig. 5** online). Notably, K14-*Angptl6* transgenic mice 8 months after birth show marked reduction in body weight and adiposity compared to controls, and this phenotype is similar to that seen in *Angptl6* transgenic mice created by driving *Angptl6* expression from the CAG promoter (**Supplementary Fig. 5**). K14-*Angptl6* transgenic mice also showed increased insulin sensitivity despite an extremely decreased WAT mass (**Supplementary Fig. 5**). These findings indicate that increasing serum AGF levels could counteract obesity and related insulin resistance, suggesting a physiological role of circulating AGF secreted from liver in antagonizing obesity.

Angptl3 is a circulating factor from liver functioning to regulate lipid metabolism[14,15]. Angptl4 is also predominantly expressed in liver and adipose tissue, and its expression is altered in nutrition and fasting, suggesting a role for Angptl4 in regulating fat metabolism[12,13]. Here, we show that AGF is a new hepatocyte-derived circulating factor counteracting high-fat-induced obesity and related insulin resistance through increased energy expenditure. Taken together with these findings, members of Angptl family function as endocrine factors with overlapping function secreted mainly from the liver to regulate metabolic homeostasis. As a next step to understand the role of Angptl family members in regulating metabolic homeostasis, identification of their cognate receptors and studies aimed at understanding their functional interactions are necessary.

In summary, we provide the first evidence that AGF directly antagonizes obesity and related insulin resistance. In addition to this direct effect, we propose that AGF-induced angiogenesis facilitates increased energy expenditure. Thus, AGF is a potential target for developing attractive pharmacological interventions counteracting obesity and related metabolic diseases.

METHODS

Gene targeting of *Angptl6*, generation of *Angptl6* transgenic mice, cell culture, transcription assays, western blot analyses and laser Doppler blood flow analysis. Please see **Supplementary Methods** online.

Blood analysis and tissue triglyceride assay. For IGTT, female mice were deprived of food 16 h and given 0.75 mg glucose per g body weight intraperitoneally; 3-month-old *Angptl6*$^{-/-}$ mice and controls and 4-month-old *Angptl6* transgenic mice and controls were used (n = 5–6 each). For IITT, female mice were given 0.75 U human insulin per kg body weight by subcutaneous injection; 3-month-old *Angptl6*$^{-/-}$ mice and controls and 4-month-old *Angptl6* transgenic mice and controls were used (n = 5–6 each). Blood was withdrawn from the supraorbital vein at indicated times. Blood glucose was measured by glucose oxidase method (Sanwa Kagaku). Serum FFA, triglyceride and cholesterol levels were determined by nonesterified fatty acid C-test, triglyceride L-type and cholesterol L-type (Wako), respectively. Plasma insulin was measured by insulin immunoassay (Eiken Kagaku).

Leptin, adiponectin and TNF-α were assayed by leptin assay kit (Linco Research Inc.), ELISA-based adiponectin immunoassay kit (Otsuka Seyaku) and ELISA-based TNF-α immunoassay kit (Techne Corporation), respectively, according to the manufacturer's instructions. Tissues were excised, weighed and homogenized. We added 500 μl of homogenates to 3 ml of methanol/chloroform at 1:2 (vol/vol). The mixture was shaken for 10 min and then centrifuged. We removed the organic layer and saved it, and re-extracted the aqueous layer with 3 ml of methanol/chloroform, and evaporated a small aliquot of the combined organic extracts. The triglyceride concentration of this aliquot was determined as described earlier.

Physiological measurements. For measurement of food consumption, 6-month-old *Angptl6*$^{-/-}$ mice and controls (n = 8 each), and 5-month-old *Angptl6*-transgenic mice and controls (n = 10 each) were housed individually. We measured consumption of food, as well as body weight, for 7 d consecutively. Mice were fed a normal chow diet (CE-2) or a high-fat diet (HFD-32) (CLEA). The high-fat diet study with 6-week-old *Angptl6* transgenic mice and controls was followed for a period of 12 weeks. Rectal temperature was monitored (6-month-old *Angptl6*$^{-/-}$ mice and controls (n = 8 each), and 5-month-old *Angptl6*-transgenic mice and nontransgenic control mice (n = 10 each)) using an electronic thermistor (Model BAT-12) equipped with a rectal probe (RET-3, Physitemp). Oxygen consumption (VO_2) was determined in 6-month-old *Angptl6*$^{-/-}$ mice and controls (n = 5 each), and 5-month-old *Angptl6*-transgenic mice and controls (n = 12 each), with an O_2/CO_2 metabolic measuring system (Model MK-5000, Muromachikikai) at 24 °C as described elsewhere[41]. Mice were kept unrestrained in the chamber for 24 h without food. We determined VO_2 when the minimum plateau shape was obtained during the light cycle, which corresponded to the period of sleep or inactivity. VO_2 is expressed as the volume of O_2 consumed per kilogram weight of lean body mass per minute.

Quantitative RT-PCR. Total RNA was isolated from the BAT and musculus gastrocnemius of mice (6-month-old *Angptl6*$^{-/-}$ mice and controls (n = 5 each), and 6-month-old *Angptl6*-transgenic mice and controls (n = 5 each)). Preparation of DNase-treated total RNA, reverse transcription, and PCR protocols were performed as previously described[8]. The oligonucleotides used for PCR are listed in **Supplementary Table 1** online. We monitored the levels of PCR products with an ABI PRISM 7700 sequence detection system and analyzed them with ABI PRISM 7700 SDS software (Applied Biosystems JAPAN Ltd). The relative abundance of transcripts was normalized to constitutive expression of 18sRNA, β-actin or HPRT mRNA.

CT scan analysis. The adiposity of mice was examined radiographically using CT (LaTheta, ALOKA) according to the manufacturer's protocol. We performed CT scanning at 2-mm intervals from the diaphragm to the bottom of the abdominal cavity.

Hepatic overexpression of AGF by adenoviral transduction. To prepare high-fat diet–induced obese mice, 8-week-old C57BL/6 female mice were fed a high-fat diet containing 32% (wt/wt) fat (HFD-32) for 12 months. Subsequently, mice with high-fat diet–induced obesity (n = 8) received 5×10^9 plaque-forming units (p.f.u.) of Ad-AGF. Serum AGF level was elevated by a single injection of Ad-AGF. For controls, mice with high-fat diet–induced obesity (n = 8) received 5×10^9 p.f.u. of Ad-GFP at the same time. We monitored body weight and food intake daily after intravenous injection of Ad-AGF and Ad-GFP. On day 16 after injection, random fed blood glucose levels were examined. Subsequently, ITT was performed. On day 20 after injection, we examined levels of serum AGF and fasting blood glucose. Subsequently, IGTT was performed.

Statistical analysis and ethical considerations. Results are expressed as the mean ± s.d. or mean ± s.e.m. Differences between groups were examined for statistical significance using Student t test or analysis of variance (ANOVA) with Fisher's PLSD test. The Ethics Review Committee for Animal Experimentation of Keio University approved the experimental protocol.

Note: Supplementary information is available on the Nature Medicine website.

ACKNOWLEDGMENTS

We thank K. Fukushima for her assistance with the experiments. This work was supported by Grants-in-Aid for Scientific Research on Priority Areas from the Ministry of Education, Science and Culture of Japan, by the Yamanouchi Foundation for Research on Metabolic Disorders and by the Mochida Memorial Foundation for Medical and Pharmaceutical Research.

COMPETING INTERESTS STATEMENT

The authors declare competing financial interests (see the *Nature Medicine* website for details).

Received 4 July 2004; accepted 25 January 2005
Published online at http://www.nature.com/naturemedicine/

1. Spiegelman, B.M. & Flier, J.S. Obesity and the regulation of energy balance. *Cell* **104**, 531–543 (2001).
2. Matsuzawa, Y., Funahashi, T. & Nakamura, T. Molecular mechanism of metabolic syndrome X: Contribution of adipokines adipocyte-derived bioactive substances. *Ann. NY Acad. Sci.* **832**, 146–154 (1999).
3. Lowell, B.B., & Spiegelman, B.M. Towards a molecular understanding of adaptive thermogenesis. *Nature* **404**, 652–660 (2000).
4. Levine, J.A., Eberhardt, N.L., & Jensen, M.D. Role of nonexercise activity thermogenesis in resistance to fat gain in human. *Science* **283**, 212–214 (1999).
5. Gale, N.W., & Yancopoulos, G.D. Growth factors acting via endothelial cell-specific receptor tyrosine kinases: VEGFs, Angiopoietins, and ephrins in vascular development. *Genes Dev.* **13**, 1055–1066 (1999).
6. Oike, Y. *et al.* Angiopoietin-related/like protein (ARPs/Angptls) regulate angiogenesis. *Int. J. Hematol* **80**, 21–28 (2004).
7. Oike, Y. *et al.* Angiopoietin-related growth factor (AGF) promotes epidermal proliferation, remodeling and regeneration. *Proc. Natl. Acad. Sci. USA.* **100**, 9494–9499 (2003).
8. Oike, Y. *et al.* Angiopoietin-related growth factor (AGF) promotes angiogenesis. *Blood* **103**, 3760–3766 (2004).
9. Kim, I. *et al.* Molecular cloning, expression, and characterization of angiopoietin-related protein. *J. Biol. Chem.* **274**, 26523–26528 (1999).
10. Camenisch, G. *et al.* ANGPTL3 stimulates endothelial cell adhesion and migration via Integrin αvβ3 and induces blood vessel formation *in vivo*. *J. Biol. Chem.* **277**, 17281–17290 (2002).
11. Ito, Y. *et al.* Inhibition of angiogenesis and vascular leakiness by Angiopoietin-related protein 4. *Cancer Res.* **63**, 6651–6657 (2003).
12. Yoon, J.C. *et al.* Peroxisome proliferator-activated receptor gamma target gene encoding a novel angiopoietin-related protein associated with adipose differentiation. *Mol. Cell Biol.* **20**, 5343–5349 (2000).
13. Kersten, S, *et al.* Characterization of the fasting-induced adipose factor FIAF, a novel peroxisome proliferator-activated receptor target gene. *J. Biol. Chem.* **275**, 28488–28493 (2000).
14. Koishi, R, *et al.* Angptl3 regulates lipid metabolism in mice. *Nat. Genet.* **30**, 151–157 (2002).
15. Inaba, T, *et al.* Angiopoietin-like protein 3 mediates hypertriglyceridemia induced by the liver X receptor. *J. Biol. Chem.* **278**, 21344–21351 (2003).
16. Evans, R.M., Barish, G.D. & Wang, Y.X. PPARs and the complex journey to obesity. *Nat. Med.* **10**, 355–361 (2004).
17. Spiegelman, B.M. & Flier, J.S. Adipogenesis and obesity: Rounding out the big picture. *Cell* **87**, 377–389 (1996).
18. Uysal, K.T., Wiesbrock, S.M., Marino, M.W. & Hotamisligil, G.S. Protection from obesity-induced insulin resistance in mice lacking TNF-α function. *Nature* **389**, 610–614 (1997).
19. Peraldi, P., Xu, M. & Spiegelman, B.M. Thiazolidinediones block tumor necrosis factor-a-induced inhibitor of insulin signaling. *J. Clin. Invest.* **100**, 1863–1869 (1997).
20. Yamauchi, T. *et al.* The fat-derived hormone adiponectin reverses insulin resistance associated with both lipoatrophy and obesity. *Nat. Med.* **7**, 941–946 (2001).
21. Berg, A.H., Combs, T.P., Du, X., Brownlee, M. & Scherer, P.E. The adipocyte-secreted protein Acrp30 enhances hepatic insulin action. *Nat. Med.* **7**, 647–653 (2001).
22. Shimomura, I., Hammer, R.E., Ikemoto, S., Brown, M.S. & Goldstein, J.L. Leptin reverses insulin resistance and diabetes mellitus in mice with congenital lipodystrophy. *Nature* **401**, 73–76 (1999).
23. Friedman, J.M. Obesity in the new millennium. *Nature* **404**, 632–634 (2000).
24. Lowell, B.B., *et al.* Development of obesity in transgenic mice after genetic ablation of brown adipose tissue. *Nature* **366**, 740–742 (1993).
25. Zurlo, F., Larson, K., Bogardus, C. & Ravussin, E. Skeletal muscle metabolism is a major determinant of resting energy expenditure. *J. Clin. Invest.* **86**, 1423–1427 (1990).
26. Kamei, Y. *et al.* PPARγ coactivator 1β/ERR ligand 1 is an ERR protein ligand, whose expression induces a high-energy expenditure and antagonizes obesity. *Proc. Natl. Acad. Sci. USA.* **100**, 12378–12383 (2003).
27. Niwa, H., Yamamura, K. & Miyazaki J. Efficient selection for high-expression transfectants with a novel eukaryotic vector. *Gene* **108**, 193–200 (1991).
28. Sierra-Honigmann, M.R. et al. Biological action of leptin as an angiogenic factor. *Science* **281**, 1683–1686 (1998).
29. Sarmiento, U., *et al.* Morphologic and molecular changes induced by recombinant human leptin in the white and brown adipose tissues of C57BL/6 mice. *Lab. Invest.* **77**, 243–256 (1997).
30. Shimomura, I. *et al.* Insulin resistance and diabetes mellitus in transgenic mice expressing nuclear SREBP-1c in adipose tissue: model for congenital generalized lipodystrophy. *Genes Dev.* **12**, 3182–3194 (1998).
31. Gavrilova, O. *et al.* Surgical implantation of adipose tissue reverses diabetes in

lipoatrophic mice. *J. Clin. Invest.* **105**, 271–278 (2000).
32. Moller, D.E. & Berger, J.P. Role of PPARs in the regulation of obesity-related insulin sensitivity and inflammation. *Int. J. Obes. Relat. Metab. Disord.* **27**, S17–S21 (2003).
33. Wu, Z., *et al.* Mechanisms controlling mitochondrial biogenesis and respiration through the thermogenic coactivator PGC-1. *Cell* **98**, 115–124 (1999).
34. Puigverger, P. *et al.* Cytokine stimulation of energy expenditure through p38 MAP kinase activation of PPARγ coactivator-1. *Mol. Cell* **8**, 971–982 (2001).
35. Puigserver, P. & Spiegelman, B.M. Peroxisome proliferator-activated receptor-γ coactivator 1α (PGC-1α): Transcriptional coactivator and metabolic regulator. *Endocr. Rev.* **24**, 78–90 (2003).
36. Wang, Y.X. *et al.* Peroxisome-proliferator-activated receptor δ activates fat metabolism to prevent obesity. *Cell* **113**, 159–70 (2003).
37. Tanaka, T. *et al.* Activation of peroxisome proliferator-activated receptor delta induces fatty acid beta-oxidation in skeletal muscle and attenuates metabolic syndrome. *Proc. Natl. Acad. Sci. USA.* **100**, 15924–15929 (2003).
38. Dressel, U. *et al.* The peroxisome proliferatior-activated receptor β/δ agonist, GW501516, regulates the expression of genes involved in lipid catabolism and energy uncoupling in skeletal muscle cells. *Mol. Endocrinol.* **17**, 2477–2493 (2003).
39. Shulman, G.I., *et al.* Cellular mechanisms of insulin resistance. *J. Clin. Invest.* **106**, 171–176 (2000).
40. Petersen, K.F. *et al.* Mitochondrial dysfunction in the elderly: Possible role in insulin resistance. *Science* **300**, 1140–1142 (2003).
41. Barger, P.M., Browning, A.C., Garner, A.N. & Kelly, D.P. p38 mitogen-activated protein kinase activates peroxisome proliferator-activated receptor α: a potential role in the cardiac metabolic stress response. *J. Biol. Chem.* **276**, 44495–44501 (2001).